nature portfolio

Peer Review File

Spinel Oxide Enables High-Temperature Self-Lubrication in Superalloys

Corresponding Author: Dr Wenjun Cai

Parts of this Peer Review File have been redacted as indicated to remove third-party material.

This file contains all reviewer reports in order by version, followed by all author rebuttals in order by version.

Version 0:

Reviewer comments:

Reviewer #1

(Remarks to the Author)
The paper ”Spinel Oxide Enables High-Temperature Self-Lubrication in Superalloys” with reference number NCOMMS-24-09031 is focused on investigating the high temperature sliding friction and wear behaviour of SLM produced Inconel 718, in as-printed and heat treated conditions, during sliding against Al2O3. The work involves detailed material characterisation, high temperature tribological characterisation, analysis of oxide layers using a large number of methods, and computational work to assess shear strength of oxides as well as oxidation thermodynamics. The overall aim of the study is to demonstrate that friction and wear control can be achieved by in-situ oxidation of a metal surface to facilitate formation of spinel-based oxide layers.
The manuscript is well-written and the work is presented in a logical and easy to follow manner. Sufficient number of relevant references are provided to motivate the need for this specific study.
The work is relevant to the field of high temperature tribology and contributes with some new insights and explanations as to why simultaneous low friction and wear can be achieved when two solid surfaces (at least one metal) slide against each other at high temperature in an oxidating environment.
However, despite the comprehensive work behind this study there are a number of aspects that will require further analysis and/or clear justification by the authors before the paper can be published. The following are the detailed questions and concerns about the work:
1. On page 2, line 60, the authors mention a “frictionless” surface. This term should be changed since a surface does not have friction. Friction is not an intrinsic material property; it is a system response when sliding against another solid material.

2. In any friction and wear test, the measured friction force and the material removal is a system response that depends on four main elements: solid body 1, solid body 2, the interfacial media, and the surrounding atmosphere. In the data provided by the authors there is no analysis at all of the Al2O3 counter body which is main shortcoming of the current work.

3. The main aspects to be addressed pertaining to the Al2O3 ball are:
a. What is the hardness if the Al2O3?
b. What is the initial surface roughness of the Al2O3 balls?
c. What does the worn surface of the Al2O3 balls look like after sliding against the AP and HT samples at the different temperatures? Any signs of wear? Material transfer? Formation of oxide layers?

4. The surface roughness of the AP and HT samples should be reported since this will have a significant effect on the initial running-in behaviour of the system.

5. If the Al2O3 ball suffers wear during the tribological test, and judging by the difference in wear scar width of the AP700 and HT700 samples this seems very likely, a number of factors will affect the resulting friction and wear response:
a. The contact area will increase and the contact pressure will reduce during the test. This will result in lower wear of the Inconel sample as well as promote easier formation of a homogenous oxide layer on the Inconel surface. I.e., the lower wear measured for HT700 may not be due to the heat treatment resulting in different oxides but rather a difference in contact geometry that preferentially forms a layered oxide structure. See mechanism description by Stott et al. [Ref: F. H. Stott, Tribology International (1998)] on how oxide layers develop and correlate to contact geometry/size and contact pressure.

b. The material removed from the Al2O3 ball will very likely be integrated into the wear scar on the Inconel surface. How will this affect the composition of the oxide layer? What will this do to the kinetics discussed in the paper pertaining to the formation of a layered oxide?

6. The high temperature hardness of the Inconel will have a significant effect on the ability of the bulk material to resist deformation during the tribological test as well as to be able to support the hard oxide layers that develop on the surface. This aspect should be discussed and also if the AP and HT materials are expected to exhibit differences in hot hardness.

7. Is there any reason for reporting the time in ms for the CoF(t)? Please comment on this.

8. In the friction graphs shown in Fig. 2a, it is clear that the frictional stability of the AP samples are better than that of the HT samples when sliding against Al2O3 at both 700 and 900°C. This should be discussed in the paper and correlated to the formation of different oxides as well as the mechanical properties of the AP and HT samples.

9. The comparison of friction data in Figure 1h is somewhat questionable since the data obtained from literature is very likely measured using different tribosystems (counter body) and different tribometers (type of motion etc.) which makes a direct comparison of the absolute values impossible. The authors are recommended to revisit this analysis and perhaps extract only the data that is obtained from tribosystems using Al2O3 as counter body.

10. The hypothesis on page 6, line 160, and page 13, line 341 stating that the periodic variation of the measured friction force is connected to a quasi-periodic structural change of the surface, explained as a constant phase transformation between the two states of spinel, is an interesting theory. However, in the reviewer's opinion this is very unlikely to be the main source of the observed fluctuations since the fluctuation period is so short that the phase transformation would need to take place several times during the contact time (if considering one point on the plate moving across the contact length created by the ball). Also, for this to occur with such repeatability from the very initial sliding is not plausible since formation of the oxide layer is not instantaneous but requires some time before it stabilise. The authors are encouraged to reevaluate this theory and consider stick-slip phenomena at the sliding interface combined with the dynamics of the test setup, e.g. stiffness of the ball holder and eigenfrequencies of the mechanical components, which are more likely to be a root cause that results in the observed vibrations/instabilities.

11. The term corundum is used in the manuscript to describe e.g. Cr2O3. This was somewhat confusing as corundum usually means Al2O3. The reviewer understands that the authors refer to the corundum structure, as a type of oxide, but encourages the authors to clarify this in the manuscript. Especially when corundum is used a standalone term.

12. The analysis of the worn surfaces shown in Supplementary Figs. 5 and 6 should be complemented with sliding direction labels as well as identification of the dominant wear mechanisms. From Fig.5 e-h it is clear that the mechanisms are very different, and this will likely play an important role in explaining the material removal from the Inconel surface as well as the friction response that is measured.

13. The hardness of the worn surfaces is only mentioned at one point on the manuscript (page 6, line 172) and a discussion in Supplementary material related to Fig. 13. There is however some interesting findings in Fig. 13 with a quite homogeneous hardness increase inside the wear track on AP700 compared to HT700. A comment on this and any correlation to the detailed descriptions of the oxide layers would be valuable.

Reviewer #2

(Remarks to the Author)
This manuscript investigates the origins of low friction behavior of Inconel 718 with a specific heat treatment. It is claimed that when testing the friction and wear behavior of this material at high temperatures (600-900°C), the friction coefficient of the heat-treated sample was found to be lower than those reported in the literature for this material previously. The authors attribute this low friction behavior to the formation of a spinel-based surface oxide, which serves to lubricate the interface. A computational approach was developed to predict oxide lubricity based on shear modulus, formation energy, cohesive energy, and phase stability. While the authors do demonstrate a potential method for predicting lower friction oxides which are stable at high temperatures using DFT, the reported friction coefficients and associated proposed mechanisms are not sound. The primary discussion for this paper focuses on the low friction result, fluctuation in the measurement, and a proposed structural mechanism, all of which stem from what is likely an incorrect interpretation from a measurement artifact. As such, I recommend rejection of this manuscript. The section below addresses these concerns in more detail.

Major Questions/Comments:
Major concern/Comment 1: The friction data shown for HT700 in Fig 2 and in the mechanism Fig 6c shows this significant variation in friction (in what appears to be a waveform), which is cyclic in nature and repeats every 1 second. During testing on the tribometer, the authors utilized a sliding speed of 10 mm/s and a stroke length of 5mm (10mm per cycle), which means that one reciprocation cycle takes 1 second. The significant friction variation occurs exactly in sync with this reciprocation, which was not addressed by the authors. These fluctuations of friction synced with cycle can be attributed to a number of things, including measurement artifacts (e.g. cross talk on signals, misaligned samples, etc.) or possibly a non-uniform, spatially variable friction coefficient, and indicates an issue with the measurement itself and not a structural/mechanistic origin. The variation in friction observed cannot be attributed to the proposed mechanism (structural change from cubic to tetragonal oxide), and is most likely due to: 1) a misalignment of the sample stage, 2) issue with

acquisition sampling, 3) heterogeneous, spatially varying friction, 4) mis-processed data or 5) other testing error. The authors point to a quasi-periodic surface structural change occurring at “timescales much shorter than the wear test”, which cause these oscillations. this is completely false; they are, in fact, exactly at the same time scale of the reciprocation cycle (which is more relevant than the wear test duration) and these fluctuations are not structural in nature. As such, this friction result and proposed mechanism are not sound.

Comment 2: In Fig 1i, the presentation of the results of this work compared to that of other reported coefficients of friction from the literature are misleading. The histograms of friction data are shown across a wide range of temperatures and different structures. Only one result from this work was reported. However, this one data point is picked off of the minimum of the friction waveform. The authors should justify this comparison as they are not comparing apples-to-apples.

Comment 3: The authors report an average friction coefficient of 0.12 with a standard deviation of 0.009 for sample HT700 (Pg 5, line 147). Figure 2 a,b shows the friction coefficient of this sample to vary between ~0.04 and 0.24, in a large waveform. How was the average and standard deviation of this measurement calculated? A variation between such a large range of friction coefficients should not result in a standard deviation as low as 0.009.
Comment 4 In the methods section, the authors state that all tests on the tribometer were carried out 3 times. The friction data shown in Fig 2 is the acquired data of one test. Was the extreme, cyclical variation observed for each test on sample HT700? How were the error bars shown for the COF data shown in Fig. 1f calculated? Again, a standard deviation value of 0.009 for a friction coefficient which varies 0.04-0.22 is not correct. Does this error bar reflect the standard deviation between the 3 separate tests performed?

Comment 5: The friction power spectrum is just dropped in the paper and not really useful or discussed. Why?

Comment 6: DFT: While I am not an expert in DFT and cannot adequately assess the merits of it, it appears that the authors were able to predict which types of oxides could produce low friction interfaces – a novel and interesting contribution. However, the issues with the friction results/reporting are significant and the results are not sufficient to support the claims made in this paper. The primary discussion of the paper focuses on a mechanistic understanding of the friction behavior which was interpreted from an unsound measurement. As such, I recommend that this paper be rejected from Nature Communications. It might be reconsidered in its parts to specialized journals, as the computational results seem powerful. The tribological experiments should be repeated and carefully interpreted.

Reviewer #3

(Remarks to the Author)
Comments for Authors

In this manuscript, Zhang et al. demonstrated low coefficient of friction (COF) at high temperatures can be achieved by controlling the oxidation on the surface of Inconel superalloy made by selective laser melting (SLM). Post-printing heat treatment led to the formation of high density interphase boundary, which promoted the formation of spinel oxides which have lower COF than other oxides. DFT calculations on shear modulus, formation energy, cohesive energy, and energy per atom under shear strain were performed to predict oxide lubricity. Based on this analysis, the authors proposed design guidelines for producing lubricious oxide with high thermal stability. Overall, the experiment and analysis are well executed and the work should be published. I have several comments for the authors:

1. Are there any surface oxide after the heat treatment? I assume there is some surface oxide as the specimen was air cooled from 954°C after solutionization (pg. 14, line 369). In that case, what is the thickness and nature of the oxide on the specimen before wear test? Without this data (XPS survey and high resolution scan of AP and HT surface, cross-sectional TEM/STEM), it is difficult to fully trace the structural origin and evolution of the lubricious spinel oxide. As it stands, it is not clear when the spinel oxide was first formed.

2. The microstructure of the surface oxide is not clearly shown in the STEM data and only dark contrast can be observed within the oxide layer on the HAADF images. For instance, what is the grain size of the surface oxide? Perhaps this can be addressed with bright field TEM imaging.

3. How does the grain size of the surface oxide layer compare to the size of the features on the phase map presented in Figure 4?

4. Pg 15, line 425, it should be Transmission electron microscopy and diffraction simulation

5. Pg 15, line 427, .. using four-dimensional scanning transmission electron microscopy (4D-STEM)

6. In standard practice of XPS, survey scans should be included for the reader better comprehend the high resolution XPS scans of the material under investigation.

Reviewer #4

(Remarks to the Author)

I co-reviewed this manuscript with one of the reviewers who provided the listed reports. This is part of the Nature Communications initiative to facilitate training in peer review and to provide appropriate recognition for Early Career Researchers who co-review manuscripts.

Version 1:

Reviewer comments:

Reviewer #1

(Remarks to the Author)
The revised paper ”Spinel Oxide Enables High-Temperature Self-Lubrication in Superalloys” with reference number NCOMMS-24-09031A is focused on investigating the high temperature sliding friction and wear behaviour of SLM produced Inconel 718, in as-printed and heat treated conditions, during sliding against Al2O3. The overall aim of the study is to demonstrate that friction and wear control can be achieved by in-situ oxidation of a metal surface to facilitate formation of spinel-based oxide layers.
The Authors have made a very thorough job with addressing all the comments and questions raised by the Reviewer. The additional high temperature hardness measurements, in-depth analysis of the Al2O3 counter-body (SEM/EDS, XPS) after the tribological tests, and the detailed analysis and explanation of the friction data has significantly improved the quality of the manuscript. The Reviewer particularly appreciates the comprehensive and pedagogical explanations/justifications provided by the authors in the Response to Reviewers Comments.
With the implementation of all these changes, the Reviewer considers the manuscript to be acceptable for publication.

Best regards,

Jens Hardell
Professor, Head Division of Machine Elements
Luleå University of Technology
Sweden

Reviewer #3

(Remarks to the Author)
The authors have addressed all of my comments with the exception of Q3.4. Pg 15, line 425, it should be Transmission electron microscopy and diffraction simulation. (pg 16, line 455 on the revised manuscript)

Response to Reviewer Comments (NCOMMS-24-09031)

We sincerely thank all reviewers for the careful reading of our manuscript and for their constructive feedback. The questions raised and suggestions provided by the reviewers have been instrumental in improving the quality of our work, and we are truly grateful for their time and effort dedicated to this review.

We provided below a detailed response to all the points raised in the reviewers' comments. Revisions made to the manuscript appear in red font for ease of visualization. We also want to point out that since we do not have a high-temperature indenter for hardness measurement, the additional high-temperature indentation experiments were performed in collaboration with Prof. Bai Cui's group at University of Nebraska-Lincoln. As a result, Md Rezwan Ul Islam, Xin Chen, and Bai Cui are now added as co-authors due to their contribution to the revised manuscript.

Revisions made are highlighted below:

1. High temperature hardness measurements are now added, including the procedure and results in Supplementary Information section 2.
2. High temperature tribological tests setup, validation, and results (including raw data) are added in Supplementary Information section 3, updated in Figures 1 and 2 of the main text.
3. Characterization results of the Al_2O_3 ball are now added in Supplementary Information section 4.
4. Discussion on material transfer is now added in Supplementary Information section 4.6.

Added figures and tables:

1. Supplementary Figures 4-17, 22-23, 27-30
2. Supplementary Table 3

Revised figures and data:

1. Figure 1e,g,h,i
2. Figure 2
3. Figure 3b,d
4. Figure 6c
5. Supplementary Figures 21
6. Source data file

Reviewer #1

Q1.1. On page 2, line 60, the authors mention a "frictionless" surface. This term should be changed since a surface does not have friction. Friction is not an intrinsic material property; it is a system response when sliding against another solid material.

Response: We completely agree that the frictional response of the surface is a result of the whole system's behavior, which not be confused as an intrinsic material's property. We have made the following revisions to clarify this point in the revised manuscript.

Original statement in the second paragraph of the introduction:

"To minimize the overall material loss at high temperatures, a wear-resistant and frictionless surface is desired."

Modified text:

"To minimize the overall material loss at high temperatures, a wear-resistant and self-lubricating surface is desired."

Q1.2. In any friction and wear test, the measured friction force and the material removal is a system response that depends on four main elements: solid body 1, solid body 2, the interfacial media, and the surrounding atmosphere. In the data provided by the authors there is no analysis at all of the Al2O3 counter body which is main shortcoming of the current work.

Response: We completely agree on the importance of the counterbody, which is Al_2O_3 ball in this work. We provide additional characterization results of the counterbody before and after each wear test using SEM and EDS. This information is now added to both the manuscript **Methods section** (for the properties of the counterbody before wear test including purity, sphericity, and Rockwell hardness) and the **Supplementary Information Section 4** (for surface morphology of the counterbody before and after wear test, and EDS mapping and composition analysis of the worn area on the Al_2O_3 ball against the Inconel samples). More details about characterization of the counterbody is also provided in the answer to the next question.

Q1.3. The main aspects to be addressed pertaining to the Al_2O_3 ball are:

a. What is the hardness of the Al_2O_3?

b. What is the initial surface roughness of the Al_2O_3 balls?

c. What does the worn surface of the Al_2O_3 balls look like after sliding against the AP and HT samples at the different temperatures? Any signs of wear? Material transfer? Formation of oxide layers?

Response: We provide additional information about the Al_2O_3 ball, as detailed below. The following information is also added to the revised manuscript and **Supplementary Materials Section 4.3-4.5.**

a. The Al_2O_3 ball was produced and supplied by Rtec Instruments, CA, USA. It has a 96-99.8 wt.% purity, Rockwell hardness of 45N (i.e. 45-kgf load) scale 83, which is comparable to alumina grade 995 with (nom.) 99.5 wt.% Al_2O_3 from other vendors (e.g. (https://www.modernceramics.com/material-properties).

   The following statement is now added to the Methods section of the paper.

   "All tests were carried out for 3 repeated times in a reciprocating ball-on-plate mode using alumina ball (Al_2O_3, diameter of 6.35 mm, 96-99.8 wt.% purity, sphericity of 99.9975%, Rockwell hardness of 45N 83) as the counterbody,"

b. The surface roughness of Al_2O_3 is primarily influenced by its porosity. The initial surface morphology of Al_2O_3 was characterized using SEM, as shown in **Supplementary Figure 28 a-b**. The porosity on the Al2O3 surface measures to be 3.84 ± 1.84 µm. When compared to the surface morphology of the ball after the wear test against Inconel samples (**Supplementary Figure 28 c-f**), it is observed that these defects within the wear contact areas are largely covered by the transfer layer. As a result, they become less significant in determining the nature of the two-body contact after the initial running-in period. The duration of the running-in period is provided in the answer to question Q1.4. Briefly, running-in observed in AP600, HT600, and HT700 samples for the first 50-100 sec, which is largely absent in AP700, P800, HT800, AP900, and HT900 samples.

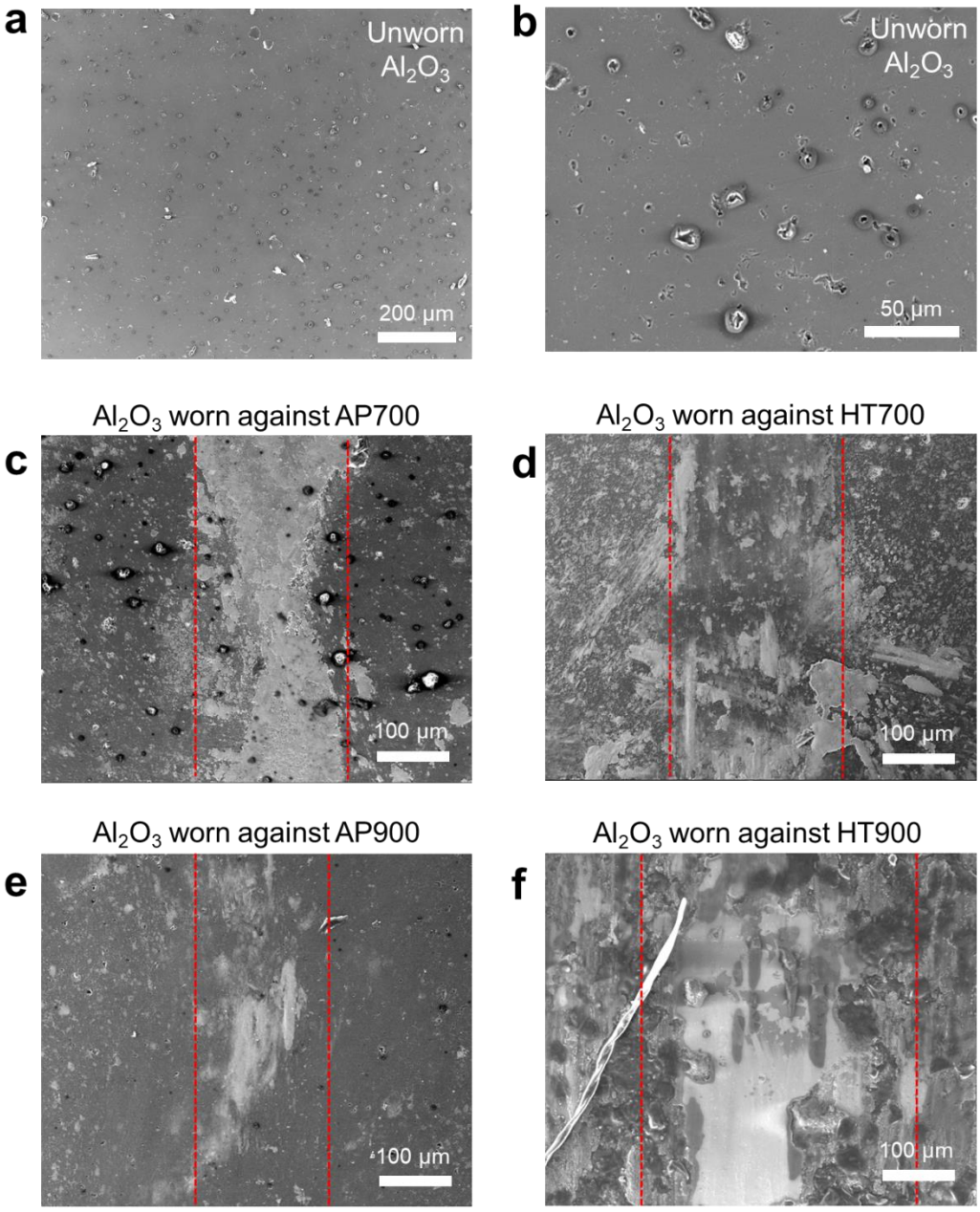

Supplementary Figure 28. Surface morphology from as-received and worn Al_2O_3 surface. SEM images of surfaces from **a-b** as-received, unworn surface of Al_2O_3 ball, and **c-f** contact area on Al_2O_3 ball after wear tests against **c** AP700, **d** HT700, **e** AP900, and **f** HT900 sample. Dashed lines in **c-f** represent the boundary of contract area.

c. In the previously shown **Supplementary Figure 28**, the surface morphology of the Al_2O_3 counterbody before (**Supplementary Figure 28a-b**) and after (**Supplementary Figure 28c-f**) high-temperature wear tests against AP700, HT700, AP900, and HT900 Inconel samples was characterized using SEM. The dashed lines in **Supplementary Figure 28c-f** indicate the boundary of the contact area. Notably, in the Al_2O_3 sample worn against the HT900, a long fiber is present near the boundary of the wear region, likely due to accidental surface contamination from tissue paper during sample handling. Since the Al_2O_3 ball was already coated with a thin layer of gold for conductivity before SEM imaging, several attempts were made to remove this fiber using compressed air, but unfortunately, these efforts were unsuccessful. Consequently, EDS mapping was performed in an adjacent region to avoid this contamination (see **Supplementary Figure 29d** below).

   In terms of surface morphology, after the wear test at 700 °C, the Al_2O_3 ball used against HT700 (**Supplementary Figure 28d**) exhibits discontinuous patches of light-colored regions within the contact area. In contrast, the ball used against AP700 shows a relatively uniform light-colored region across the entire contact area. Additional EDS mappings of these two surfaces (**Supplementary Figure 29a-b**) reveal that these light-colored regions have lower concentrations of Al and higher concentrations of Ni, Cr, Fe, and Nb compared to the unworn regions, which contain only Al and O.

   Quantitative compositional analysis from EDS point analysis at five random locations within these light-colored areas (as shown in **Supplementary Figure 30**) indicates concentrations of approximately 5.4-8.7 at.% Cr, 5.1-13 at.% Fe, 6.8-11.8 at.% Ni, 0.3-1.4 at.% Nb, 4.4-7.8 at.% Al, and 33.6-46.2 at.% O. This suggests that these materials were primarily transferred from the Inconel sample surface to the Al_2O_3 ball during the high-temperature wear test. The surface morphologies and material transfer on the ball also correlate well with the wear track depth profiles on the Inconel surfaces (**Supplementary Figures 32b-c**), where the HT700 sample shows shallow and flat wear profiles, and the AP700 sample displays deeper and curved profiles. At 900 °C, the Al_2O_3 ball tested against HT900 shows a wider wear track compared to that tested against the AP900 sample (**Supplementary Figures 28e-f**). Notably, the ball used against AP900 has the smallest contact width among all samples, which is consistent with the wear depth profiles observed on the Inconel samples (**Supplementary Figures 32b-c**).

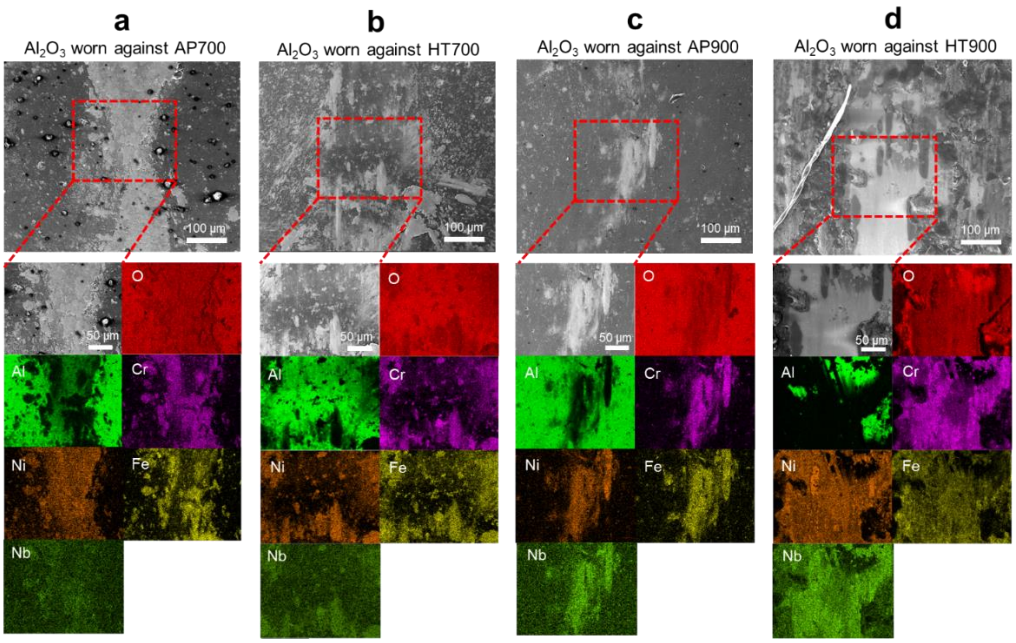

Supplementary Figure 29. Surface morphology and elemental mappings from worn Al_2O_3 surface. SEM images and corresponding EDS mappings of Al_2O_3 ball after wear test against **a** AP700, **b** HT700, **c** AP900, and **d** HT900 sample.

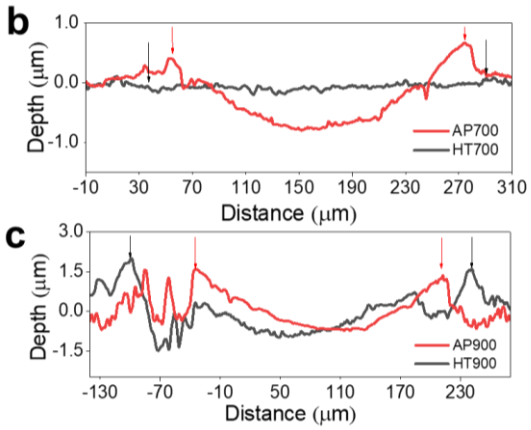

Supplementary Figure 32. Worn surface morphology and nanomechanical properties. b,c Surface profiles measured perpendicular to the sliding direction of worn surfaces of AP700, HT700, AP900, and HT900. Arrows in **b, c** indicate the edge of wear track.

a Al_2O_3 worn against AP700

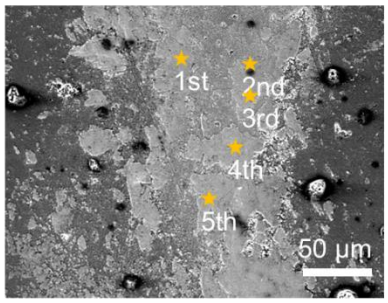

	Cr	Fe	Ni	Nb	Al	O
1st	8.6	9.8	10.7	N/A	8.2	46.0
2nd	7.6	12.0	8.1	N/A	9.6	45.0
3rd	9.6	16.4	5.7	0.3	6.3	46.5
4th	5.1	11.0	7.0	0.4	8.4	46.3
5th	7.2	16.0	7.1	0.3	6.6	46.3
Avg. (at.%)	**7.6**	**13.0**	**7.7**	**0.3**	**7.8**	**46.0**
SD (at.%)	1.51	2.68	1.67	0.05	1.22	0.53

b Al_2O_3 worn against HT700

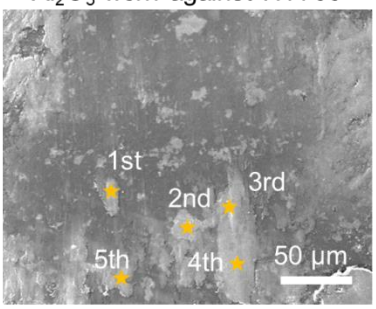

	Cr	Fe	Ni	Nb	Al	O
1st	4.3	3.3	10.7	0.8	8.3	38.7
2nd	11.6	8.1	9.4	1.8	1.7	44.5
3rd	7.1	6.5	11.9	1.1	2.6	45.4
4th	7.3	6.7	14	1.3	1.9	43.4
5th	5.7	6.2	12.9	0.8	7.7	44.4
Avg. (at.%)	**7.2**	**6.2**	**11.8**	**1.2**	**4.4**	**43.3**
SD (at.%)	2.45	1.57	1.61	0.37	2.93	2.38

c Al_2O_3 worn against AP900

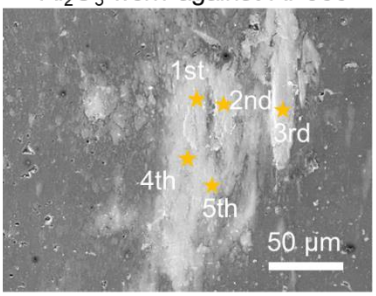

	Cr	Fe	Ni	Nb	Al	O
1st	8.2	7.2	8	1.6	6.1	45.6
2nd	10.4	6.1	7.4	2	6.3	47.4
3rd	11.1	7.4	11.3	1.4	2	46.2
4th	5.8	5.3	7.8	1.1	13.5	45.2
5th	8	9	10.9	1.1	5	46.6
Avg. (at.%)	**8.7**	**7.0**	**9.1**	**1.4**	**6.6**	**46.2**
SD (at.%)	1.89	1.26	1.67	0.34	3.79	0.77

d Al_2O_3 worn against HT900

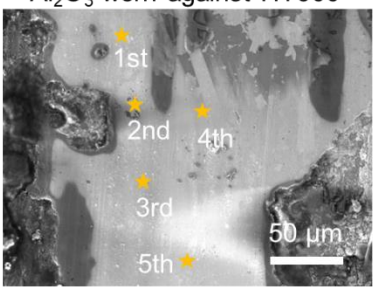

	Cr	Fe	Ni	Nb	Al	O
1st	3.6	7.4	10.3	0.7	0.4	30.8
2nd	1.5	0.4	1.7	0.2	21	33.3
3rd	7.8	7.6	4.7	1.2	2.9	32.6
4th	4.8	5.2	9.4	0.8	5.4	36.2
5th	9.5	5	7.7	1.5	2.1	34.9
Avg. (at.%)	**5.44**	**5.12**	**6.76**	**0.88**	**6.36**	**33.6**
SD (at.%)	2.88	2.59	3.17	0.44	7.5	1.864

Supplementary Figure 30. EDS composition analysis from worn Al_2O_3 surface. SEM images (left) and compositions (right) in atomic percent (at.%) of Al_2O_3 ball after wear test against **a** AP700, **b** HT700, **c** AP900, and **d** HT900 sample. Stars in SEM images (left) mark the EDS point analysis locations listed in the table (right). Avg. and SD in the table represent average and standard deviation from all measurements respectively.

To confirm that material transfer primarily occurs from the Inconel sample to the Al_2O_3 ball, additional XPS depth analysis, including the Al element, was performed on the unworn and worn surfaces of the Inconel samples, as shown in **Supplementary Figure 21**. Note that as shown in **Supplementary Figure 21a-b**, in the unworn bulk Inconel samples, XPS analysis of the top surface (averaging the composition from sputter time 0 to 10 min) shows AP and HT samples already have an Al concentration of 1.47 at.% and 1.19 at.% respectively. After wear tests at 700 °C, these is not much Al concentrated on the Inconel sample surface, as evidenced by the lower Al content (0.45-0.65 at.%) in the surface oxide layer, as compared to the slightly higher Al content (1.05-3.49 at.%) observed at 900 °C. This finding is consistent with the TEM cross-section analysis (see Figure 4b in the paper) where there are some Al clusters ~ 200 nm within the surface oxide of HT900 sample. Such very small amount of Al detected on the surfaces of the AP900 and HT900 samples indicate either there is some material transfer from the ball to the Inconel surface or enhanced diffusion of Al from the Inconel bulk to the surface. At this point, we are not able to rule out either of the two possibilities. Nonetheless, based on these characteristics, we conclude that in the Inconel/Al_2O_3 contact pair, material transfer primarily occurs from the Inconel surface to the Al_2O_3 ball.

Finally, it is worth noting that at 700 °C, the HT700 sample has a higher hardness than the AP700 sample (see high temperature hardness data in the **Response to Reviewer 1 Q1.6 and Supplementary Figure 5**), which would result in a smaller contact area per Archard's law [1]. However, the opposite is observed in this case. Both the ball and the Inconel sample show a relatively large contact area, characterized by discontinuous rather than continuous material transfer between the two surfaces. This suggests that the oxide layer formed on HT700 is lubricious, and its formation on the discrete contact areas leads to a relatively large yet flat worn surface on the Inconel, contributing to the low wear rate of HT700. During dry sliding wear, the initial contact area is often small during the running-in period, which typically develops into more severe wear over time, resulting in deep and curved surface profiles, such as those observed on AP700 (**Supplementary Figure 32b**). The fact that the contact area remains patchy on the Al_2O_3 ball used against HT700 (**Supplementary Figure 32b**) further confirms the lubricity of the oxides formed at the contact points, which helps lubricate the sample surface and prevents it from progressing into more severe wear.

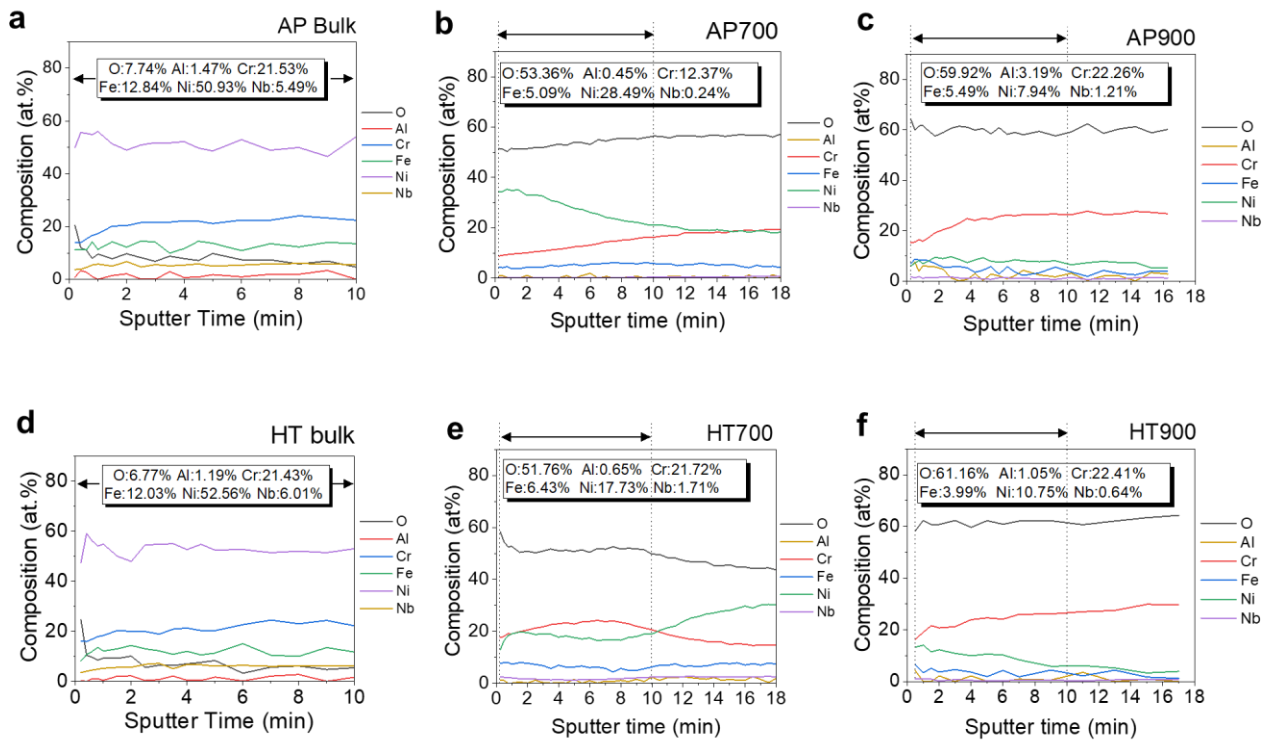

Supplementary Figure 21. XPS depth profile of Inconel 718 samples. XPS line profiles of O, Al, Cr, Fe, Ni, and Nb from the (a, d) unworn bulk samples, and (b-c, e-f) wear track region of AP700, HT700, AP900, and HT900 samples. Sputter time 0 corresponds to the outermost surface and higher sputter time corresponds to deeper location below the surface. The inset composition in **a-f** shows the average compositions (at.%) from the first 10 min of sputter time in all samples.

Q1.4. The surface roughness of the AP and HT samples should be reported since this will have a significant effect on the initial running-in behavior of the system.

Response: We provide additional characterization of the surface roughness of the AP and HT samples in **Supplementary Figure 17** below. Briefly, the samples underwent progressive griding using 240-320-400-600-800-1200 grit sand papers, followed by polishing using 1 μm Al_2O_3 colloidal suspension solution prior to the tribological testing. The unworn AP sample and HT sample has Ra values of 1.7 and 2.56 μm respectively. Some porosity can be seen on both samples, which are likely keyhole and lack-of-fusion defects from laser-based additive manufacturing.

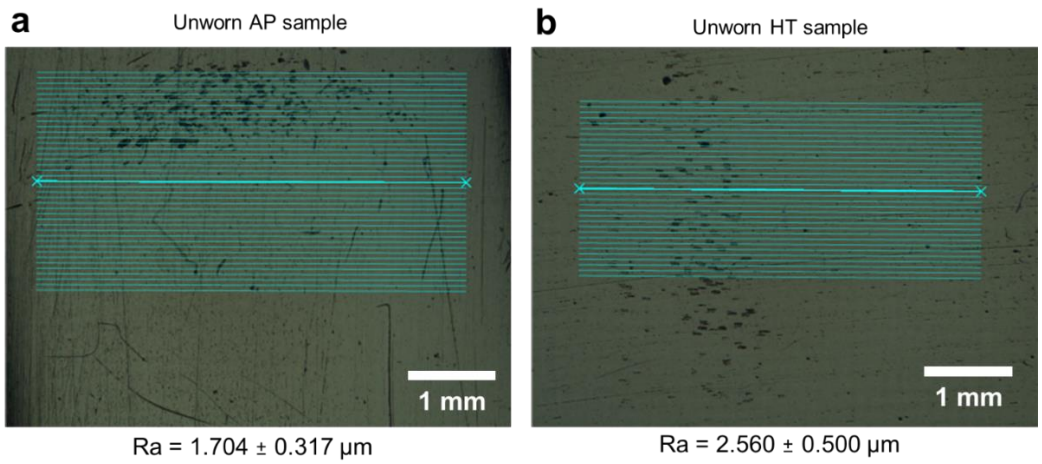

Supplementary Figure 17. Surface roughness from AP and HT samples before wear test. Optical images of unworn **a** AP and **b** HT Inconel 718 samples with scan regions overlayed for surface roughness measurement. The reported Ra values are calculated as the average of the surface's peaks and valleys.

Q1.5. If the Al_2O_3 ball suffers wear during the tribological test, and judging by the difference in wear scar width of the AP700 and HT700 samples this seems very likely, a number of factors will affect the resulting friction and wear response:

a. The contact area will increase and the contact pressure will reduce during the test. This will result in lower wear of the Inconel sample as well as promote easier formation of a homogenous oxide layer on the Inconel surface. I.e., the lower wear measured for HT700 may not be due to the heat treatment resulting in different oxides but rather a difference in contact geometry that preferentially forms a layered oxide structure. See mechanism description by Stott et al. [Ref: F. H. Stott, Tribology International (1998)] on how oxide layers develop and correlate to contact geometry/size and contact pressure.
b. The material removed from the Al2O3 ball will very likely be integrated into the wear scar on the Inconel surface. How will this affect the composition of the oxide layer? What will this do to the kinetics discussed in the paper pertaining to the formation of a layered oxide?

Response: We sincerely thank the reviewer for pointing out this very important paper by Stott that we overlooked. We have added this reference [2] and related discussion in the Results section of the revised manuscript. To summarize the key points in the Stott's paper, we agree with all the claims on the oxidation mechanism, where "low sliding speed, low load and high rates of oxidation helps to reduce wear". However, while Stott's paper summarizes wear behavior trend from 400-

600°C, our work provides additional insight into a higher temperature range from 600-900 °C that shows a different behavior, especially those at 700 °C due to the formation of a special crystal structure and microstructure of the surface oxide due to heat treatment of the as-printed material, which is the key novelty of this work. In other words, all the tests performed in this work under 600-900 °C results in the formation of a glaze layer (i.e. a continuous oxide layer as noted by Stott), yet the glaze layer formed at 700 °C on the heat treated samples has different mechanical property and results in different friction and wear response, as compared to those not heat-treated.

Per Stott's opinion that 'During low-speed, reciprocating sliding, under conditions where debris can be retained between the contacting surfaces, such debris can be compacted into the surfaces, giving effective wear protection." [2] This is indeed in agreement with our observation in this work. Additionally, Stott claimed that "the main effects of increasing temperature are that the rate of generation of wear debris particles, particularly oxide debris is increased, more debris particles are involved in establishment of the compacted wear-protective layers and the compaction of such particles into a surface layer is facilitated." This claim was formulated based on the wear data presented from room temperature to 600 °C in Stott's paper (as shown in **Figure R1a** below), which is completely different from what we observed from a higher temperature range from 600-900°C, where the wear rate of both AP and HT samples increased when the temperature increased from 600 to 900 °C.

In terms of material transfer between the two contacting bodies, as discussed in the previous question, based on the top surface XPS analysis (**Supplementary Figure 21**), as well as TEM analysis of the oxide composition from cross-sectional Inconel samples after wear (**Figure 4**), we did not detect any significant material transfer from the Al_2O_3 ball to the Inconel surface at 700 and 900 °C.

In terms of different contacting geometry, as shown earlier in the wear track morphology on both the Al_2O_3 ball and Inconel surface at 700 °C and 900 °C, the larger and flatter contact area in HT700 sample distinguishes it from all other cases. Notably, the HT700 contacting surface is even larger than that of AP700. As shown later in the hardness data **(Supplementary Figure 5),** HT700 has a higher hardness than AP700, which is often assumed to result in smaller contact area, should there be no oxide layer present. Based on these discussion above, we believe that (1) oxide reactively formed on Inconel surface is mainly affecting the frictional response and contact geometry, and (2) the low COF and wear rate of HT700 is mainly due to that lubricious oxide formed on Inconel as a result of heat treatment, while others form oxides that are more abrasive. The above discussion is concisely summarized in the revised manuscript Results section.

[REDACTED]

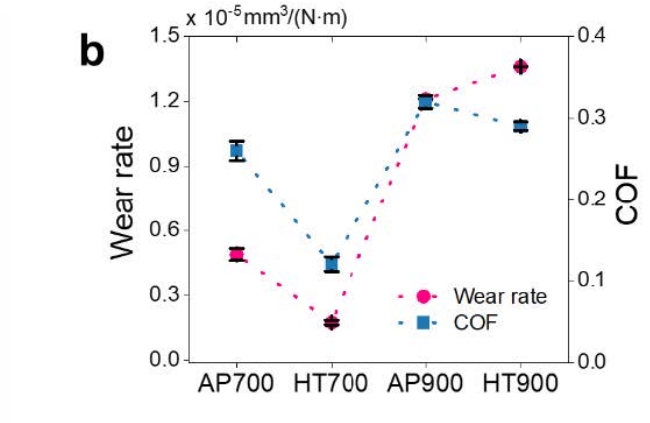

Figure R1. a. Figure 11a from Stott's paper (ref[2]) and **b** summary of wear rate and COF from this work at 700 ^{o}C (AP700 and HT700) and 900 ^{o}C (AP900 and HT900).

Q1.6. The high temperature hardness of the Inconel will have a significant effect on the ability of the bulk material to resist deformation during the tribological test as well as to be able to support the hard oxide layers that develop on the surface. This aspect should be discussed and also if the AP and HT materials are expected to exhibit differences in hot hardness.

Response: We performed additional hardness tests at four temperature points (20 °C, 600 °C, 700 °C, and 800 °C) using a diamond indenter with high-temperature indentation equipment (Manufacturer: Rtec-Instrument, Model: MFT5000, Serial: RTECH3010) in an argon environment. These results are now added to Supplementary Information Section 2. **Supplementary Figure 4** shows the photo of the machine and the test setup. The maximum achievable temperature, limited by the equipment, was 800 °C. Four indentations were made at each temperature point to determine the average hardness and standard deviation. A 30 N load was applied for 10 seconds during each indentation. Following the indentations, the samples were cooled in an argon environment. Once the samples reached room temperature, the diagonal dimensions of the indents were measured using a microscope on a separate microhardness testing device (Manufacturer: ITW Test & Measurement GmbH, Model: Tukon 2500-3):.

The Vickers Hardness (HV) was calculated using the following equations:

$$HV = constant \times \frac{test\ force\ (F)}{surface\ area\ of\ the\ indent} = 0.102 \times \frac{2Fsin\frac{136^{o}}{2}}{d^{2}} = 0.1891 \times \frac{F}{d^{2}}, \quad (1)$$

$$d = \frac{d_1+d_2}{2} \text{ (average diagonal length).} \quad (2)$$

The Vickers Hardness (HV) was then converted to hardness in GPa using the following equation:

$$\text{Hardness (GPa)} = 0.009807 \times \text{Vickers Hardness (HV)} \quad (3)$$

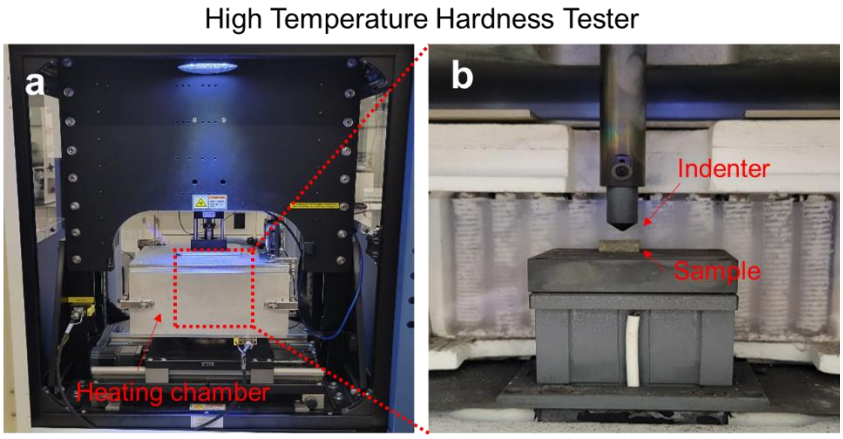

Supplementary Figure 4. High temperature indentation equipment. a Photo of the heating chamber of the indentation machine. **b** A view of the indenter and the Inconel sample.

Supplementary Figure 5 presents the results for HT and AP samples, with representative indent images shown in **Supplementary Figures 5b and 5c**. The measurements at room temperature align with the results shown in Supplementary Information Section 5. At all elevated temperatures tested, the HT samples exhibited higher hardness than the AP samples.

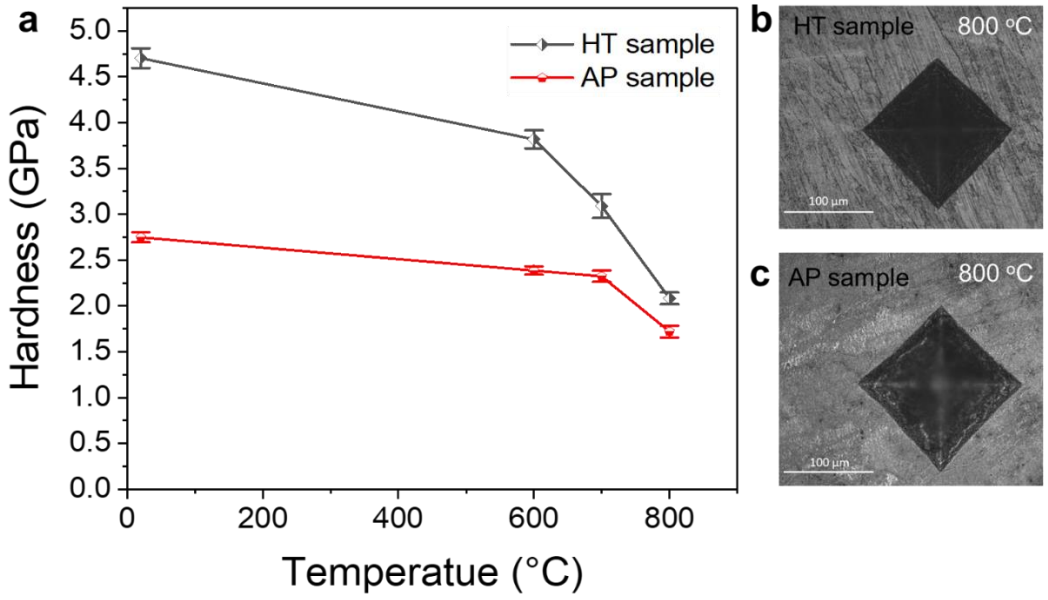

Supplementary Figure 5. a. High-temperature hardness of (unworn) as-printed (AP) and heat-treated (HT) Inconel 718 samples. Indent SEM images of b HT and c AP sample tested at 700 °C.

Q1.7. Is there any reason for reporting the time in ms for the CoF(t)? Please comment on this.

Response: The time step is chosen in the tribometer controlling software with a high sampling rate to allow subsequent power spectrum analysis of COF data to help understand the friction kinetics [3-5]. In the literature, similar or even higher sampling rate (e.g. 10 MHz = 10x 10^6 Hz) was selected [6]. In our experiment, the reciprocal wear test is done at a frequency of 1 Hz, we thus chose a sampling rate of 1 ms (10^{-3} sec). After transforming the COF(t) data into a power spectrum, we analyzed the frequency components. The raw data for COF of all samples are now provided in the source data excel file. To minimize confusion, the raw COF data is plotted using second (s) instead of millisecond (ms) in **Figure 2** of the paper.

Supplementary Figure 14 shows the power spectrum of raw COF data for the 700 °C and 900 °C wear tests. Typically, in dry sliding wear with stick-slip, the self-organized criticality in COF results in a linear relationship in its power spectrum [3-5]. This is indeed observed in AP700, AP900 and HT900 samples. However, the HT700 sample's COF(t) power spectrum exhibits large fluctuations from 0.1 Hz (10^{-1} Hz) to 1 Hz (10^0 Hz) that deviates from the linear slope of the higher frequencies (above 1 Hz), suggesting the presence of an instability in this system, which could possibly be due to phase transitions between the cubic and tetragonal spinel phases in the surface oxide layer. Previously, Yu et al. [7] reported similar breakdown of COF power law due to phase transformation and structural relaxation in metallic glass.

In **Supplementary Figure 14 and 15**, it is also noted that in the power spectrum of the wear tests performed at 1 Hz, prominent peaks at and above 1 Hz reflects the test itself. Similar patterns can be found in the literature [8, 9], where the lowest frequency sharp peak precisely corresponds to sample spinning, the subsequent peaks being its harmonics. Additionally, the 1/f noise was identified as a low frequency pattern below 0.01 Hz [9]. Therefore, to investigate wear-driven phase transition, we focus on frequencies in the 0.1-1 Hz range, potentially driven by the reciprocal movement. At a given location on the wear track, if the phase transition is driven by the sliding wear at 1 Hz, we assume that such phase transition at this location have a period larger than 1 second (1/f). Phase transitions could manifest in various modes with different periods. First, partial phase transitions within 1 second may result in total transfer frequencies lower than 1 Hz. Second, location on the wear track influences the transition periods. The center point in the stroke length experiences scratching every 0.5 seconds, while edge points may encounter 0.1-second and 0.9-second intervals (see **Supplementary Figure 8a-b**). For these reasons, the 0.1-1 Hz range power spectra should be most relevant regarding the phase transitions.

From an energy perspective, both stick-slip and phase transitions occur at energetically favorable points. Stick-slip happened at shorter times, while phase transitions (e.g., between spinel and corundum phases or between high and low symmetry spinel phases) on the wear track is driven by the sliding frequency, which is 1 Hz in the current work. Thus phase transition is expected to occur at lower than 1 Hz frequencies while stick-slip at higher than 1 Hz frequencies. In other words, the stick-slip and phase transition events likely coexist, but in different frequency domains. Given that a stress of 3.88 GPa is enough for spinel-corundum transition and 0.5 GPa is enough for the Jahn-Teller effect at ideal situation from DFT calculations, the above phase transitions could occur during the wear test.

To better investigate the influence of wear test frequency on the frictional response, and to verify that the sharp peaks at 1 Hz is indeed introduced by the testing frequency itself, we conducted additional tests at 2 Hz using heat-treated Inconel and stainless steel 316 as a reference under the same testing condition (8 N load, 700 ºC, Al_2O_3 counter body). These results are summarized in **Supplementary Figures 15-16**. Indeed, for 2 Hz tests using either Inconel or stainless steel samples, the sharp peak shifts to 2 Hz, as indicated by the green dashed lines. With the 2 Hz wear test, it is also noticed that the phase transition feature in HT700 sample disappeared. In other words, the slope at frequencies below the test frequency is different for that above the test frequency at 1 Hz, but the same at 2 Hz. This could be due to less oxidation at higher sliding frequency, which results in less noticeable phase transition, hence resumes the traditional linear relationship in the power spectrum. Nonetheless, more work is required to systematically investigate the frequency-dependent instabilities due to stick-slip and phase transitions in the future.

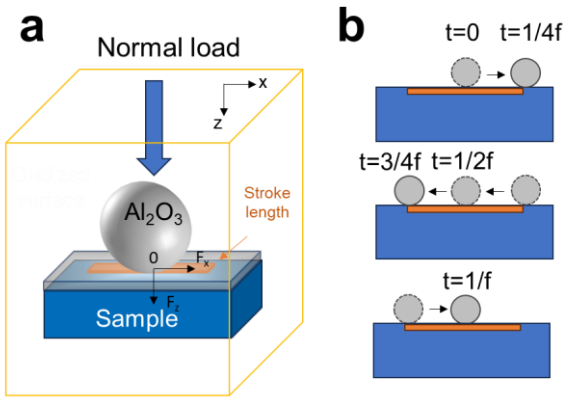

Supplementary Figure 8. a Schematic of the reciprocal motion between the ball and the Inconel sample. **b** Schematic showing the ball's position on the sample as a function of time, with f representing the testing frequency.

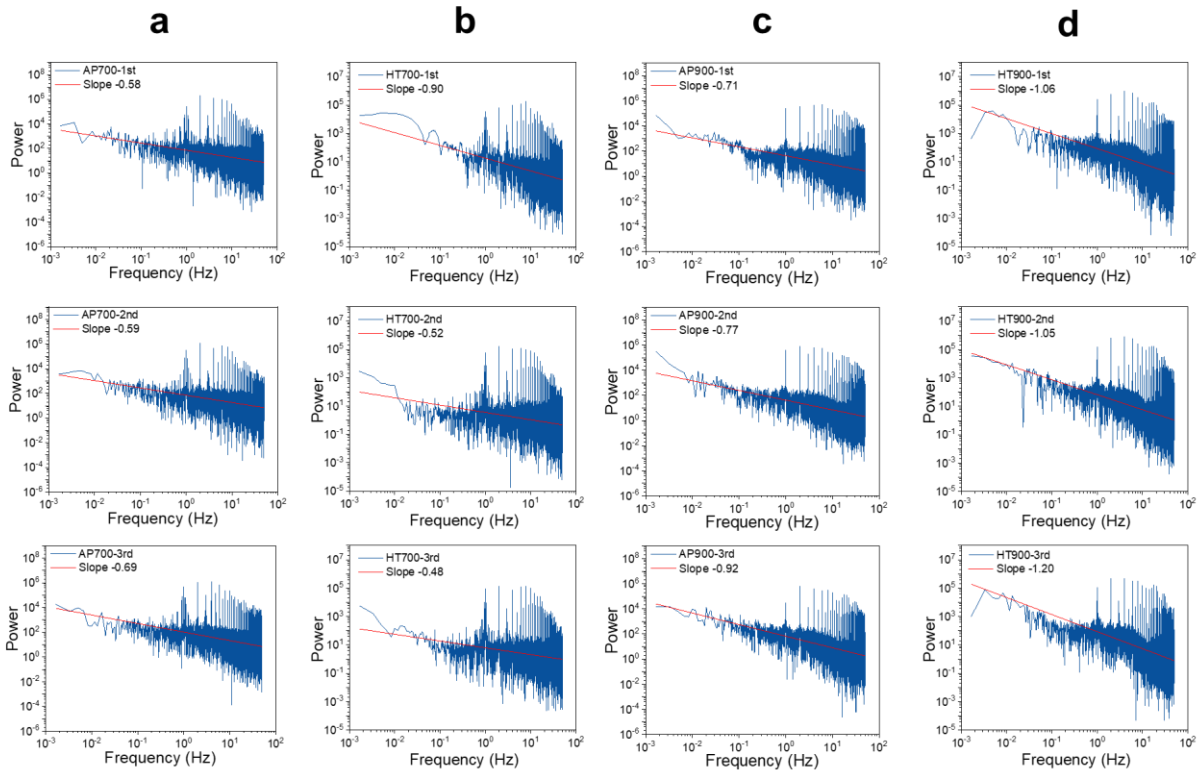

Supplementary Figure 14. Power spectra of raw COF data for a AP700, **b** HT700, **c** AP900, and **d** HT900 samples. 1st, 2nd, and 3rd represent three repeated tests.

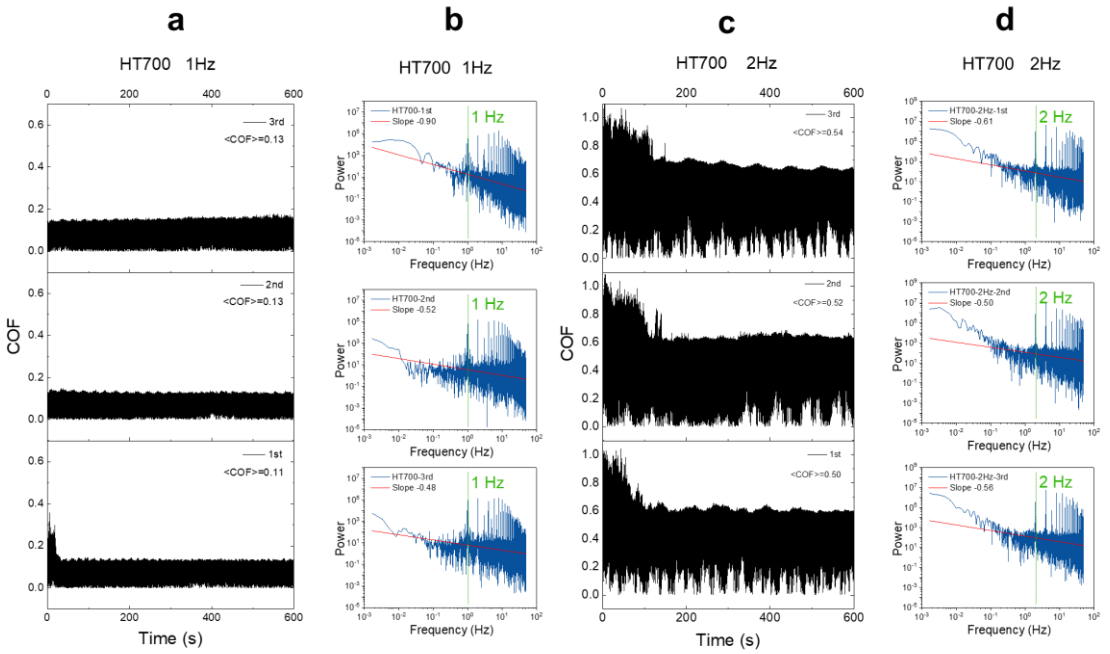

Supplementary Figure 15. Raw COF data as a function of testing frequency. a,c COF and **b,d** power spectrum of HT700 sample. 1st, 2nd, and 3rd represent three repeated tests.

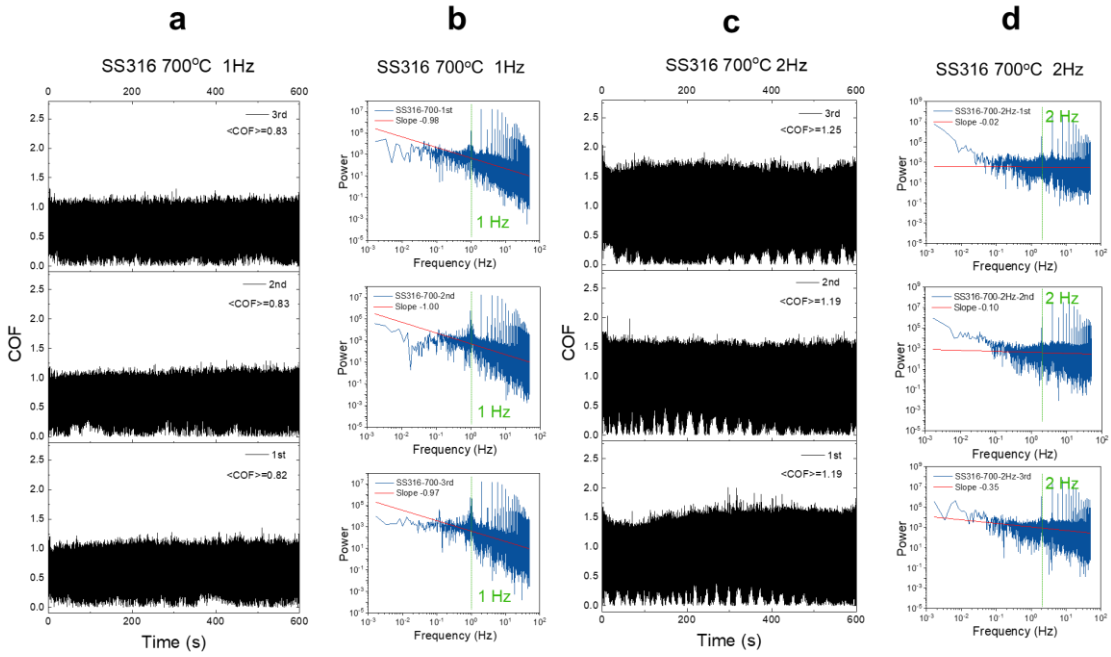

Supplementary Figure 16. Raw COF data as a function of testing frequency. a,c COF and **b,d** power spectrum of stainless steel 316 at 700 °C. 1st, 2nd, and 3rd represent three repeated tests.

Q1.8. In the friction graphs shown in Fig. 2a, it is clear that the frictional stability of the AP samples are better than that of the HT samples when sliding against Al2O3 at both 700 and 900°C. This should be discussed in the paper and correlated to the formation of different oxides as well as the mechanical properties of the AP and HT samples.

Response: Thank you for pointing this out. We provide the raw data for the frictional force (F_x) and normal force (F_z) for both AP700 vs. HT700 and AP900 vs. HT900 samples below. There is no apparent difference in frictional stability between the AP vs. HT samples. The main difference is due to its different surface lubricity in HT700, as discussed in the responses to questions Q1.5.

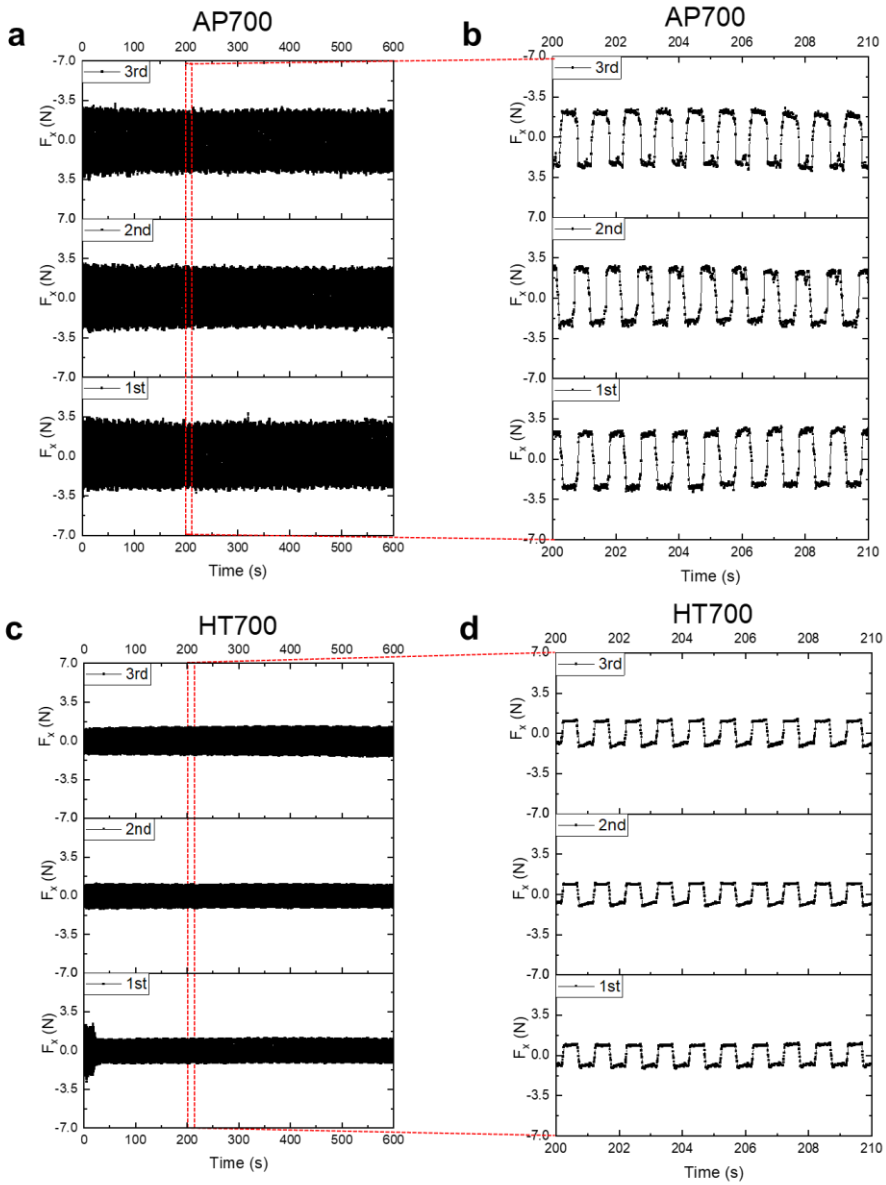

Supplementary Figure 9. Raw data of the frictional force (F_x). a,c Raw data (not processed by the RTECviewer software) of frictional force (F_x, as defined in **Supplementary Figure 8a**) of AP700 and HT700. F_x from 200 to 210 seconds of **b** AP700 and **d** HT700 sample. 1st, 2nd, and 3 rd represents three repeated tests.

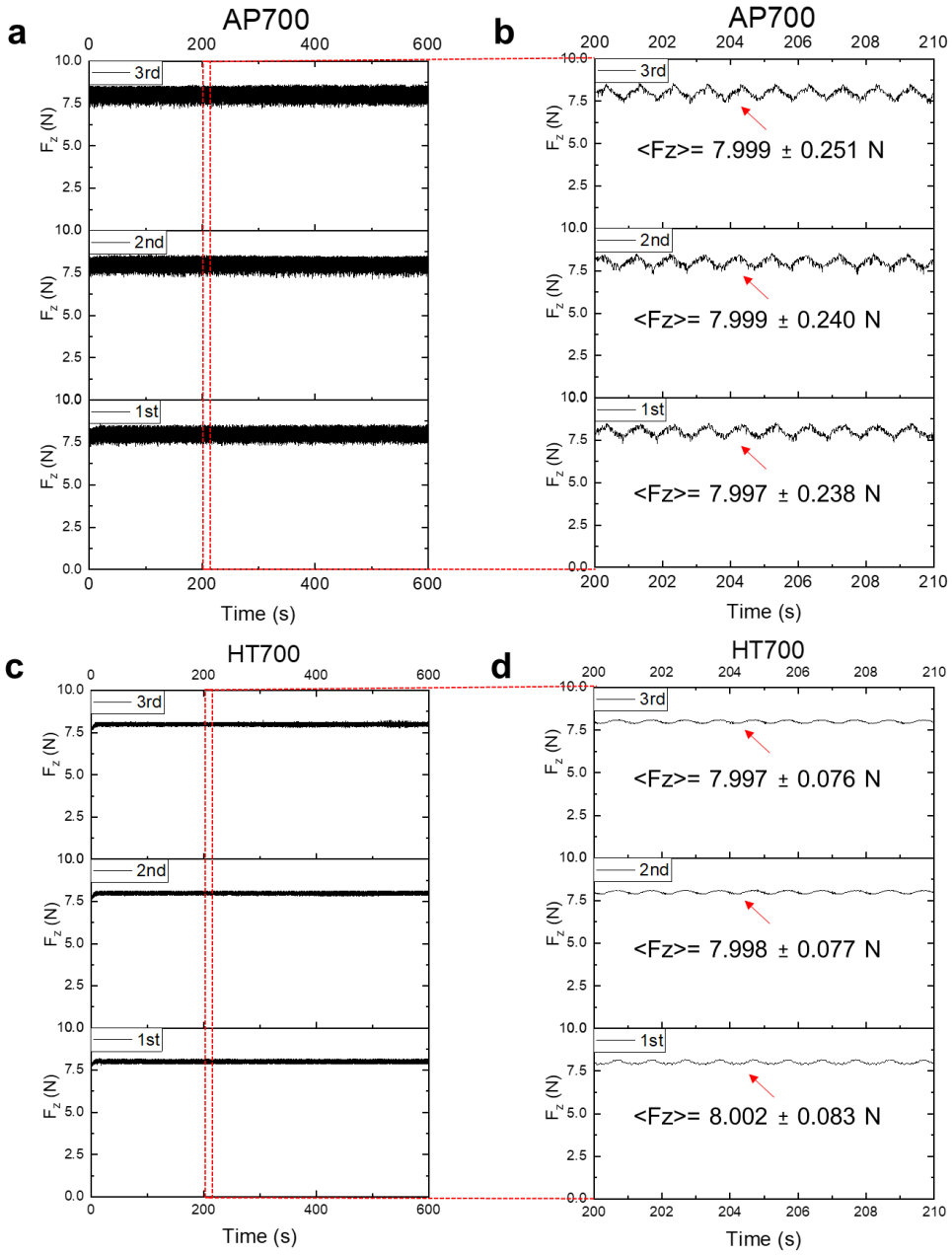

Supplementary Figure 10. Raw data of the frictional force (F_z). a,c Raw data (not processed by the RTECviewer software) of normal force (F_z, as defined in **Supplementary Figure 8a**) of AP700 and HT700. F_z from 200 to 210 seconds of **b** AP700 and **d** HT700 sample. Values in < > from **b, d** represent average values of F_z from the entire test (600 sec). 1st, 2nd, and 3 rd represents three repeated tests.

Q1.9. The comparison of friction data in Figure 1h is somewhat questionable since the data obtained from literature is very likely measured using different tribosystems (counter body) and

different tribometers (type of motion etc.) which makes a direct comparison of the absolute values impossible. The authors are recommended to revisit this analysis and perhaps extract only the data that is obtained from tribosystems using Al2O3 as counter body.

Response: We agree. We revised this figure to only focus on data using Al_2O_3 as the counter body. Fig. 1h-i shows the modified plot, showing that oxide type alone does not determine lubricity, leading to our discussion on oxide layer structure in the next section. For metal oxides with halite, spinel, and corundum structures, the coefficient of friction (COF) typically ranges widely from 0.12 to 0.5.

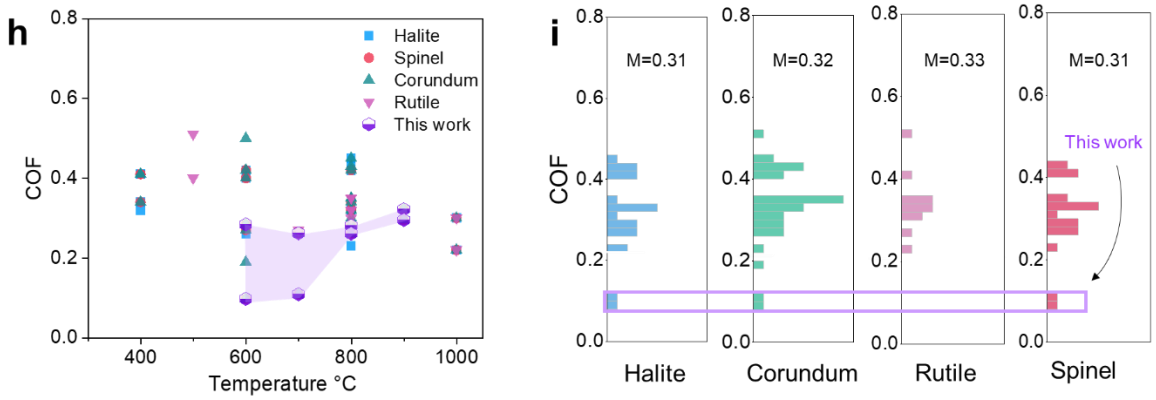

Figure 1. h. Summary of COF from literature using Al_2O_3 as counterbody (source data are provided as a Source Data file) and this work. For surface with more than one oxide type, all oxides are plotted as overlapping points in **h**. **i.** COF histogram of various oxides (halite, corundum, rutile, and spinel). M in **i** represent average value of the COF.

Q1.10. The hypothesis on page 6, line 160, and page 13, line 341 stating that the periodic variation of the measured friction force is connected to a quasi-periodic structural change of the surface, explained as a constant phase transformation between the two states of spinel, is an interesting theory. However, in the reviewer's opinion this is very unlikely to be the main source of the observed fluctuations since the fluctuation period is so short that the phase transformation would need to take place several times during the contact time (if considering one point on the plate moving across the contact length created by the ball). Also, for this to occur with such repeatability from the very initial sliding is not plausible since formation of the oxide layer is not instantaneous but requires some time before it stabilise. The authors are encouraged to reevaluate this theory and consider stick-slip phenomena at the sliding interface combined with the dynamics of the test setup, e.g. stiffness of the ball holder and eigenfrequencies of the mechanical components, which are more likely to be a root cause that results in the observed vibrations/instabilities.

Response: Thank you for this insightful point. Indeed, considering both phase transition and stick-slip phenomena can provide a more comprehensive explanation [6]. When answering both this question and question 2.1 by reviewer 2, we discovered that the somewhat sine wave form of COF is due to the RTECviewer software processed the raw COF to minimize the influence of near-zero COF values whenever the motion is switched. More details about the COF data processing is provided in the **answer to Q2.1.** As shown in the revised **Figure 2** below, the raw data for COF (not those processed by RTECviewer software in the original Figure 2) is provided. Among the four samples (AP700, HT700, AP900, and HT900), HT700 exhibited the lowest average COF of 0.11. The large amplitude in the COF data is attributed to the reciprocal motion of the wear test, which causes periodic oscillations in the frictional force (F_x) between positive and negative values (Figure 2c). This results in a near-zero COF every time the motion changes direction, approximately every 0.05 seconds (with a sliding frequency f = 1 Hz). **Figure 2b** shows examples of these oscillations in the COF data for AP700 and HT700. More details on the raw data for the frictional force (F_x), normal force (F_z), and COF for all samples, as well as repeated test results, are provided in Supplementary Information Section 3.

We performed Fourier transformation to obtain the power spectrum of this raw COF data, as shown previously in **Supplementary Figure 14**. Power spectrum analysis can be used to reveal information about the stick-slip behavior [3-5]. From an energy perspective, both stick-slip and phase transitions occur at energetically favorable points. Stick-slip happened at shorter time, while phase transitions (e.g., between spinel and corundum phases or between high and low symmetry spinel phases) on the wear track is driven by the sliding frequency, which is 1 Hz in the current work. Thus phase transition is expected to occur at lower than 1 Hz frequencies while stick-slip at higher than 1 Hz frequencies. In other words, the stick-slip and phase transition events likely coexist, but in different frequency domains. Given that a stress of 3.88 GPa is enough for spinel-corundum transition and 0.5 GPa is enough for the Jahn-Teller effect at ideal situation from DFT calculations, the above phase transitions could occur during the wear test. Nonetheless, more work is required to systematically investigate the frequency-dependent instabilities due to stick-slip and phase transitions in the future. As a results of the above considerations, we removed all discussions about the hypothesis about the variation of COF is related to phase transformation, as well as the statement about the breakdown of power law in the revised paper.

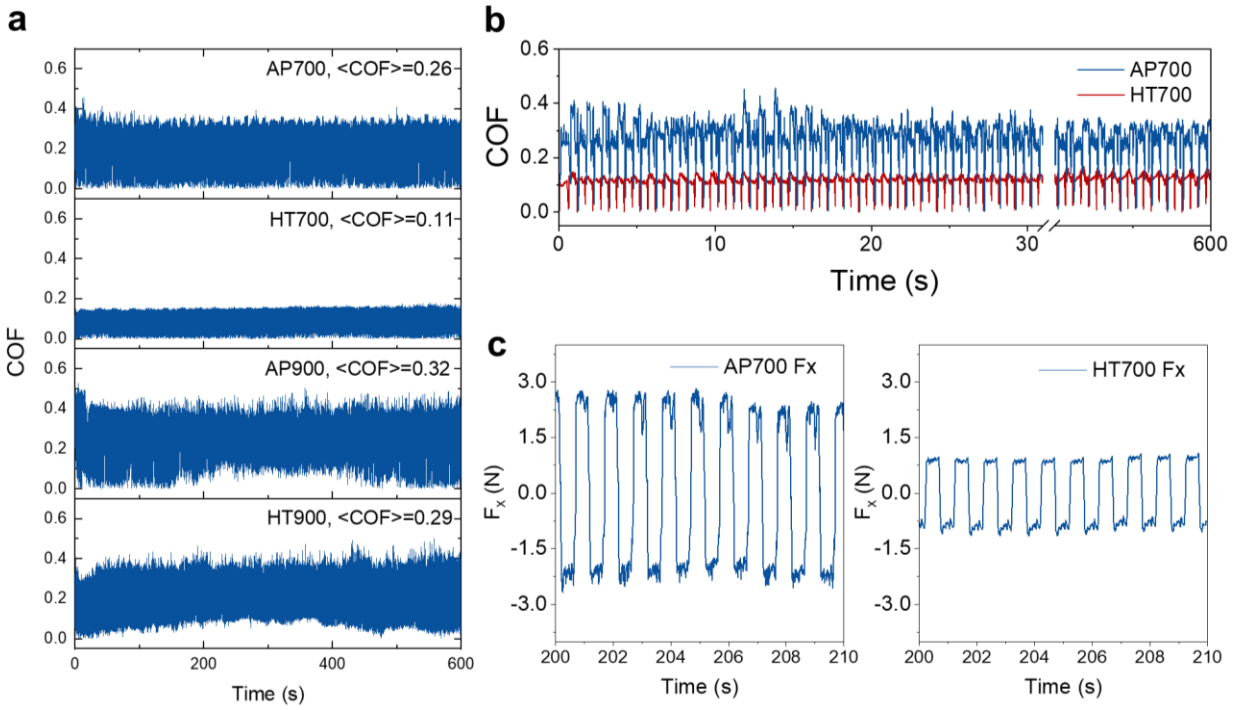

Figure 2. Temporal evolution of COF and friction force F_x. a COF of AP and HT samples from 700 and 900 ^oC. The unit of time is second (s). **b** COF of AP700 vs. HT700, **c** Frictional force (F_x) for AP700 and HT 700 samples from 200-210 s.

Q1.11. The term corundum is used in the manuscript to describe e.g. Cr2O3. This was somewhat confusing as corundum usually means Al2O3. The reviewer understands that the authors refer to the corundum structure, as a type of oxide, but encourages the authors to clarify this in the manuscript. Especially when corundum is used a standalone term.

Response: Thank you for pointing this out. We revised accordingly. The term 'corundum' is either deleted or replaced by 'corundum-structured' in the revised paper.

Q1.12. The analysis of the worn surfaces shown in Supplementary Figs. 5 and 6 should be complemented with sliding direction labels as well as identification of the dominant wear mechanisms. From Fig.5 e-h it is clear that the mechanisms are very different, and this will likely play an important role in explaining the material removal from the Inconel surface as well as the friction response that is measured.

Response: We have labeled the sliding directions in both figures. In all cases, the oxide layer, also known as glaze layer is present and protects the surface from developing into severe wear, which

corresponds to the '*Low-speed reciprocating sliding at elevated ambient temperatures'* condition per Stott's paper [2]. Based on the differences in wear rate, we labeled the wear mechanism to be mild oxidational wear at 700 ^{o}C (with wear rate on the order of 10^{-6} mm3/(N*m)) and moderate oxidational wear at 900 ^{o}C (with wear rate on the order of 10^{-5} mm3/(N*m)) [10]. Outside the wear region, the unworn region at 900 ^{o}C for both HT and AP samples shows greater signs of oxidation, as indicated by the higher surface roughness in **Supplementary Figures 18c-d**. Within the wear track, our cross-sectional TEM (**Figure 4**) and SEM (**Supplementary Figure 19**) shows that the oxide layer thickness is less than ~ 0.5-1 µm at 700 ^{o}C and ~ 2-4 µm at 900 ^{o}C.

As previously observed in the surface analysis of Al_2O_3, material transfer predominantly occurs from the oxidized Inconel surface to the ball, suggesting that the wear debris mainly originates from the oxide layer on Inconel. **Supplementary Figure 18e-h** shows a smooth wear track surface morphology in HT700 sample, consistent with its low COF, where the oxide acts as a lubricant layer, aligning with Stott's [2] 'wear-protective layer.' In the worn regions of HT700, grooves in the sliding direction are primarily due to substrate deformation under shear stress. Conversely, the wear region of AP700 shows higher oxygen content (**Supplementary Figure 18i**) compared to the unworn area, likely due to the agglomeration, compaction, and/or sintering of oxidized wear debris on the track. This accumulated oxide layer has not reached the critical thickness for spallation, remaining largely intact on the wear surface. However, unlike HT700, this oxide accumulation does not reduce the wear rate due to the abrasive nature of the oxide formed. Despite this, the wear rates of AP700 and HT700 remain within the same order of magnitude (~10^{-6} mm^3/(N*m)), classifying them as mild oxidative wear. For AP900 and HT900, the wear track regions have similar oxygen concentrations as the unworn areas (**Supplementary Figure 18k-l**), indicating a balance between wear debris compaction and removal. At these higher temperatures, both oxidation and material removal rates are increased compared to those at 700 °C, leading to their classification as moderate oxidative wear. As the paper primarily focuses on frictional response, this discussion on wear mechanisms is detailed in Supplementary Information Section 4.1.

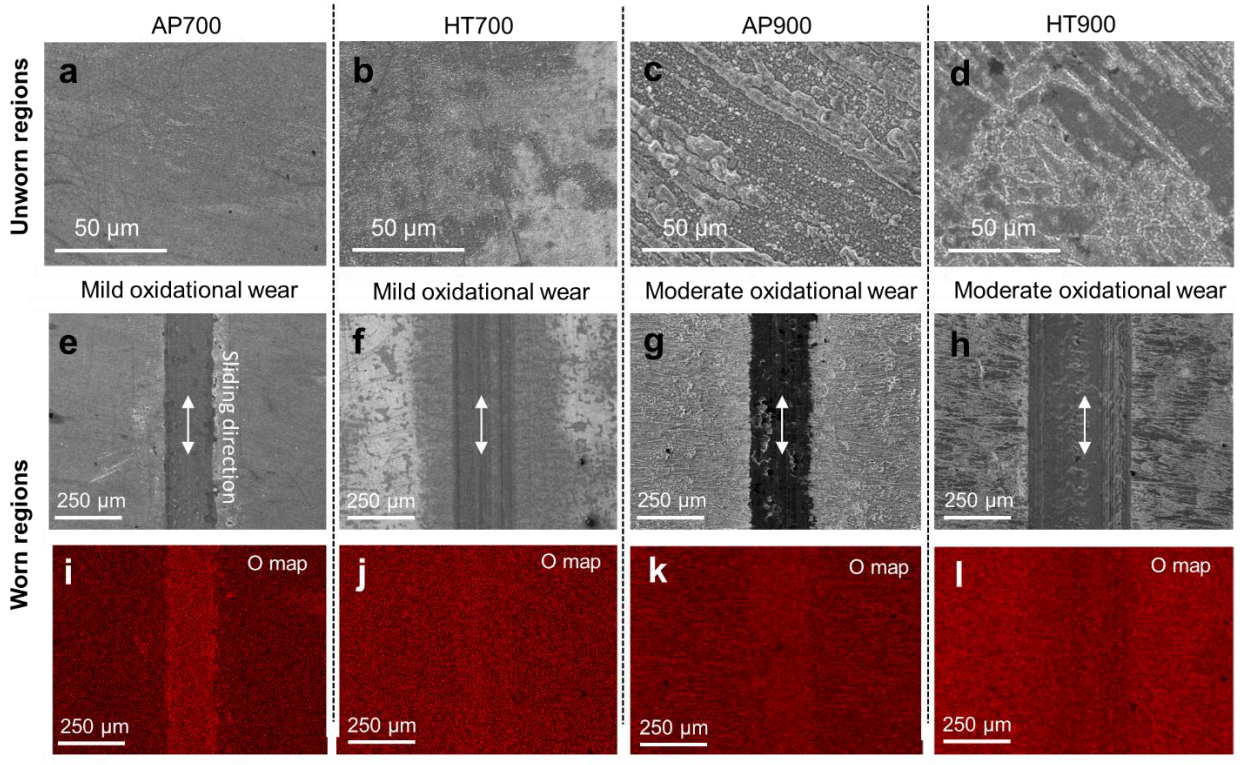

Supplementary Figure 18. Surface morphology from unworn and worn regions on Inconel 718 samples. SEM images of surfaces from **a-d** unworn and **e-h** regions, and **i-l** the corresponding oxygen elemental maps of AP700, HT700, AP900, and HT900 samples. Arrows in **e-h** represent the sliding direction.

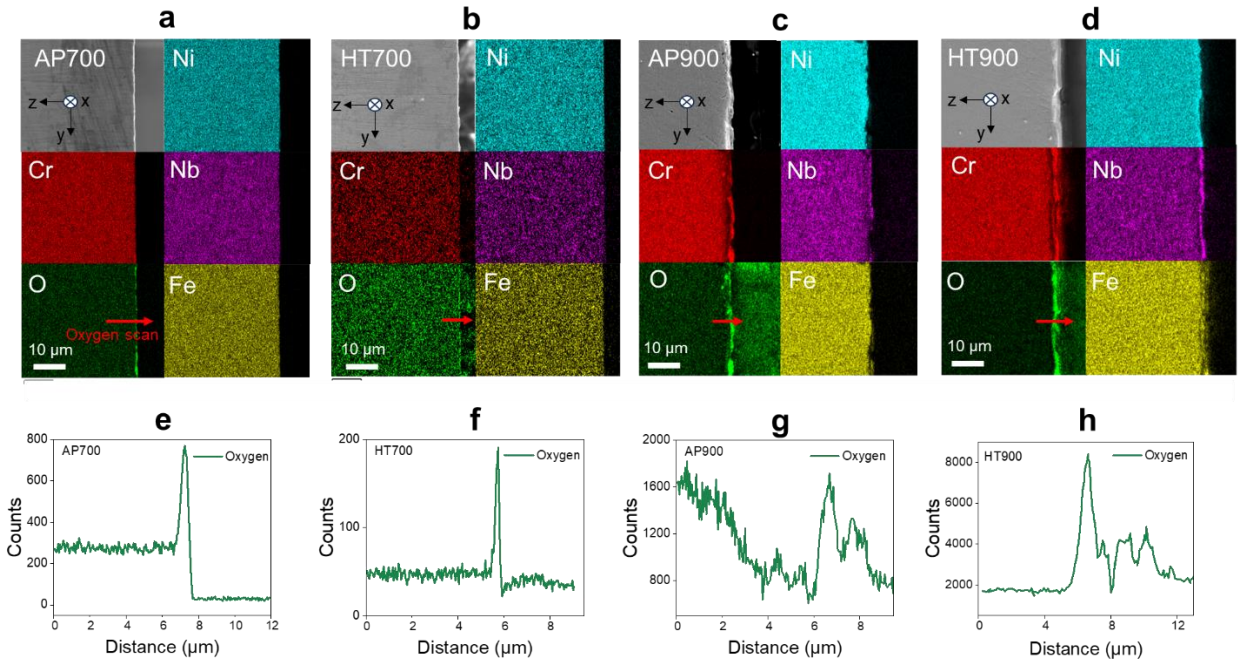

Supplementary Figure 19. Characterization of worn surface oxide layer of Inconel 718 samples. SEM image and corresponding elemental maps of **a** AP700, **b** HT700, **c** AP900, and **d** HT900 cross-sectional sample**s. e-h** The corresponding oxygen elemental maps from the arrow directions in **a-d**. x- and z- in the inset of **a-d** indicate the sliding and normal direction respectively, as defined in Supplementary Figure 8a.

Q1.13. The hardness of the worn surfaces is only mentioned at one point on the manuscript (page 6, line 172) and a discussion in Supplementary material related to Fig. Q1.13. There is however some interesting findings in Fig. 13 with a quite homogeneous hardness increase inside the wear track on AP700 compared to HT700. A comment on this and any correlation to the detailed descriptions of the oxide layers would be valuable.

Response: Thank you for this suggestion. As shown in **Supplementary Table 3** [12], oxides with a corundum structure have a hardness range of 986-3270 kg/mm², while those with a spinel structure range from 425 to 713 kg/mm². Spinel-structured oxides generally exhibit lower hardness compared to corundum-structured oxides. This trend is also observed in shear modulus, which is similarly related to bond strength. For example, $NiCr_2O_4$ has a lower shear modulus than Cr_2O_3, consistent with their hardness differences. Nano-indentation tests on the wear tracks reveal hardness values of 7.46 GPa for HT700, 8.69 GPa for AP700, 15.12 GPa for HT900, and 15.96 GPa for AP900, with HT700 showing the lowest hardness. Given that the indentation depths are under ~ 400 nm, these results likely reflect the mechanical response of the oxide layers. Such discussion is now added to Supplementary Information section 6.1.

Reported hardness of oxides

Supplementary Table 3. Data for hardness and oxide crystal structure from Ref [11].

Oxide Type	Crystal Structure	Hardness (kg/mm^2)
Fe_3O_4	spinel structure	690
Co_3O_4	spinel structure	713
α-Fe_2O_3	corundum structure	986-1219
Cr_2O_3	corundum structure	1820-3270
α-Al_2O_3	corundum structure	2160

Reviewer #2

Q2.1. The friction data shown for HT700 in Fig 2 and in the mechanism Fig 6c shows this significant variation in friction (in what appears to be a waveform), which is cyclic in nature and repeats every 1 second. During testing on the tribometer, the authors utilized a sliding speed of 10 mm/s and a stroke length of 5mm (10mm per cycle), which means that one reciprocation cycle takes 1 second. The significant friction variation occurs exactly in sync with this reciprocation, which was not addressed by the authors. These fluctuations of friction synced with cycle can be attributed to a number of things, including measurement artifacts (e.g. cross talk on signals, misaligned samples, etc.) or possibly a non-uniform, spatially variable friction coefficient, and indicates an issue with the measurement itself and not a structural/mechanistic origin. The variation in friction observed cannot be attributed to the proposed mechanism (structural change from cubic to tetragonal oxide), and is most likely due to: 1) a misalignment of the sample stage, 2) issue with acquisition sampling, 3) heterogeneous, spatially varying friction, 4) mis-processed data or 5) other testing error. The authors point to a quasi-periodic surface structural change occurring at "timescales much shorter than the wear test", which cause these oscillations. this is completely false; they are, in fact, exactly at the same time scale of the reciprocation cycle (which is more relevant than the wear test duration) and these fluctuations are not structural in nature. As such, this friction result and proposed mechanism are not sound.

Response: We sincerely thank the reviewer for pointing out this important question. We provide additional information to clarify this point, including the following aspects:

1) We provide raw data of the COF from three repeated tests for all samples in this paper. See 'COF raw data' tab in the Source data file.
2) We re-plot the raw data of COF instead of the ones generated using the tribometer's default software setting, the latter of which was used in the original submission to result in the sine-shaped waveform.
3) We bench mark our machine using stainless steel 316, and duplicated the wear response from the literature using identical wear testing condition.
4) We also provide additional information about our tribology instrument setup and sample mounting photos.
5) Most importantly, we provide a comparison of the raw vs processed COF data, including a python code to visualize the processing algorithm. More details about this analysis and our conclusion is discussed next.

In the original submission, the COF curves in Figure 2 were plotted using the RTECviewer software of the tribometer (Rtec MFT-5000). When evaluating this data again, we discovered that the raw COF data has been processed by the default algorithm of RETCviewer software (Version 1.4) to output Fx (frictional force), Fz (normal force) and COF at each point in time by integrating

all data points from the previous 0.5 sec. In reciprocal wear, it is important to note that for a test conducted at a frequency of f, the period for the ball to move back and forth once and return to its initial position will take a time of 1/f, as illuastrated in **Supplementary Figure 8a,b**. In this work, f = 1 Hz, so that the period is 1 sec. Thus the raw data of F_x (the frictional force) fluctuates btween a positive and negative value when the ball swithches direction in the reciprocal motion, resemebling a square wave form, as illuastrated in **Supplementary Figure 8d,e**. **Supplemantery Figure 9 and 10** shows a close look of such oscilation of the normal (F_z) and frictional force (F_x) due to this cyclic motion for AP700 and HT700 samples from three repeated tests.

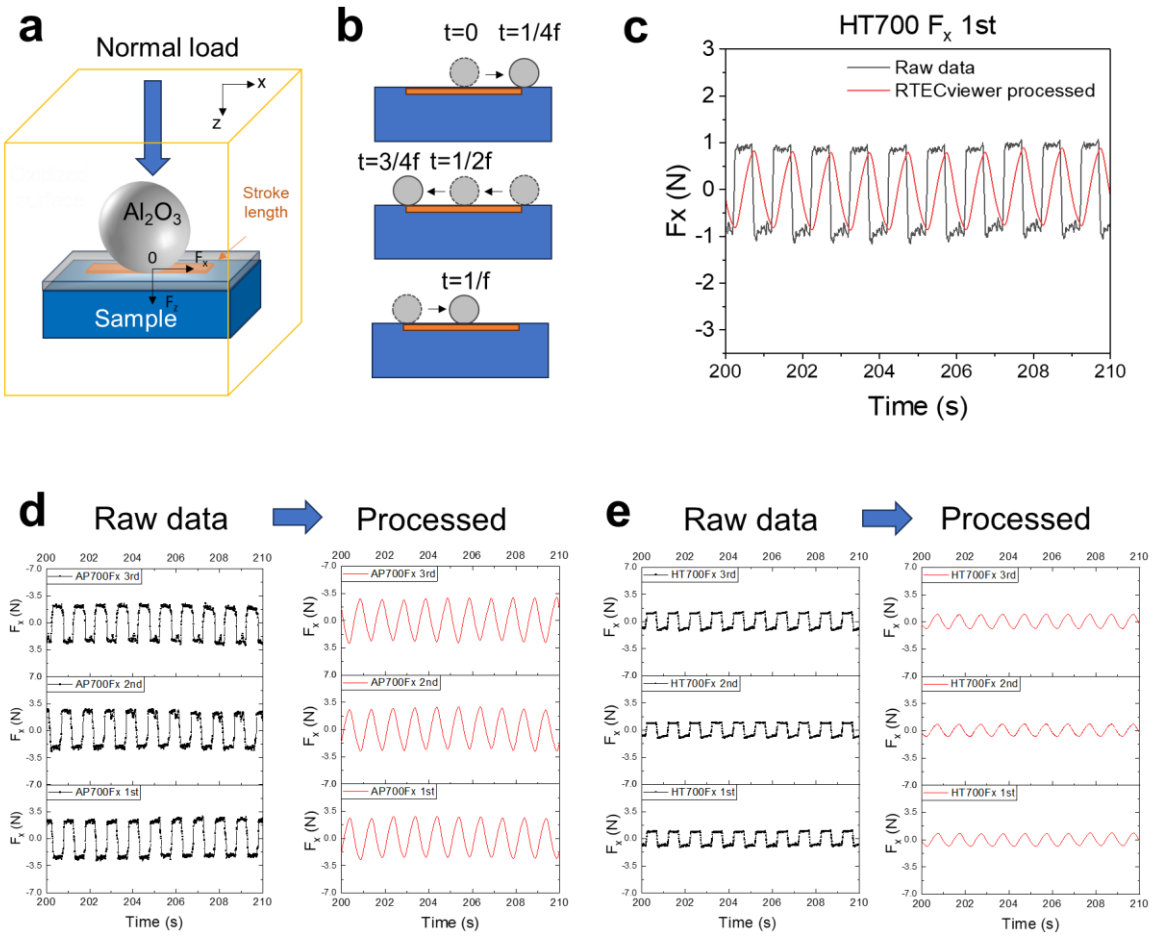

Supplementary Figure 8. Comparison of raw and processed data. a Schematic of the reciprocal motion between the ball and the Inconel sample. **b** Schematic showing the ball's position on the sample as a function of time, with f representing the testing frequency. **c** Example of raw versus RTECviewer software-processed COF data for the HT700 sample from 200 to 210 seconds. Examples of raw versus RTECviewer software-processed friction force (F_x, as defined in **a**) for the **d** AP700 and **e** HT700 samples from 200 to 210 seconds. The total duration of the wear test for both samples is 600 seconds. 1st, 2nd, and 3rd in **d** represents three repeated tests.

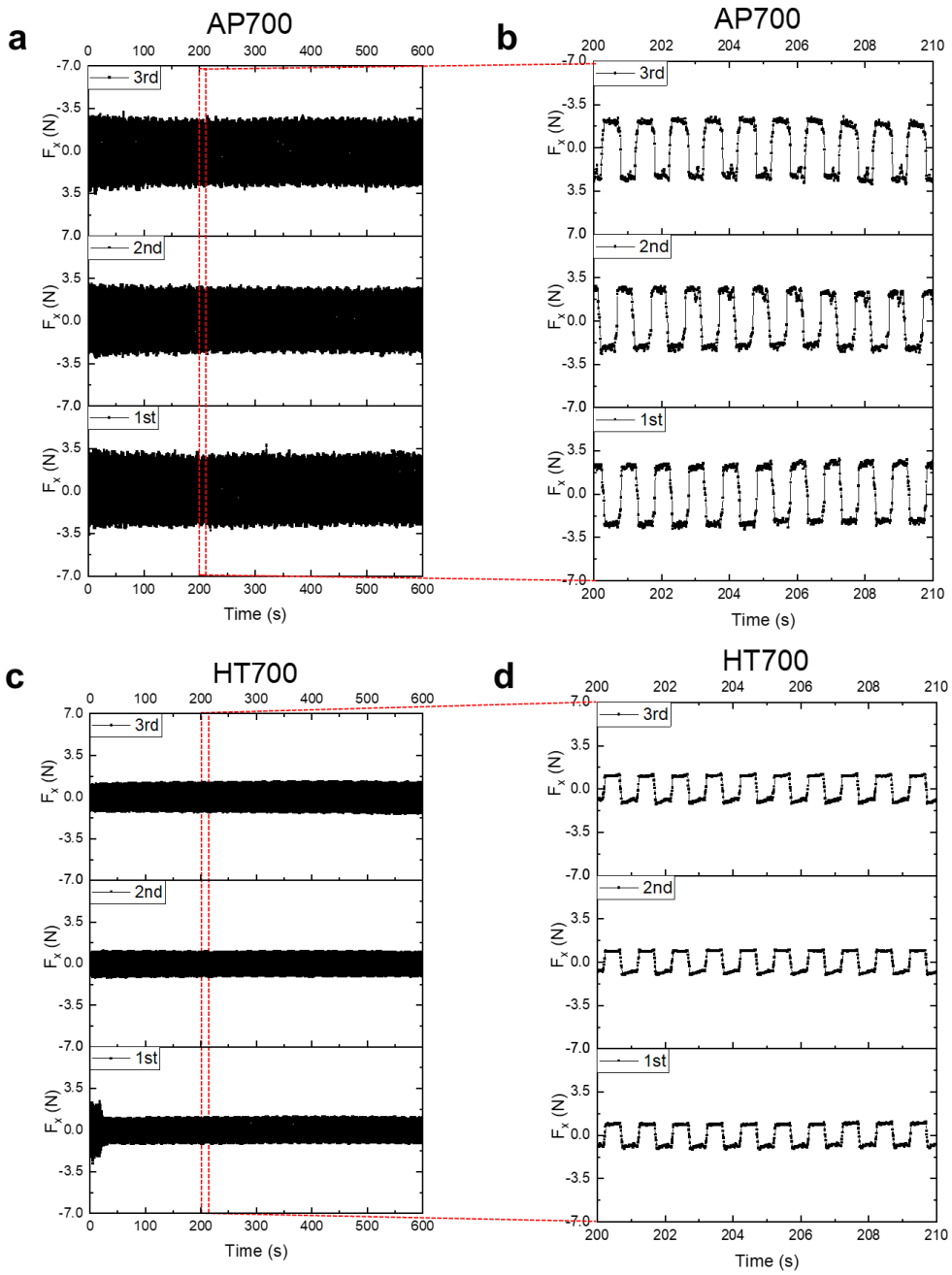

Supplementary Figure 9. Raw data of the frictional force (F_x). a,c Raw data (not processed by the RTECviewer software) of frictional force (F_x, as defined in **Supplementary Figure 8a**) of AP700 and HT700. F_x from 200 to 210 seconds of **b** AP700 and **d** HT700 sample. 1st, 2nd, and 3rd represents three repeated tests.

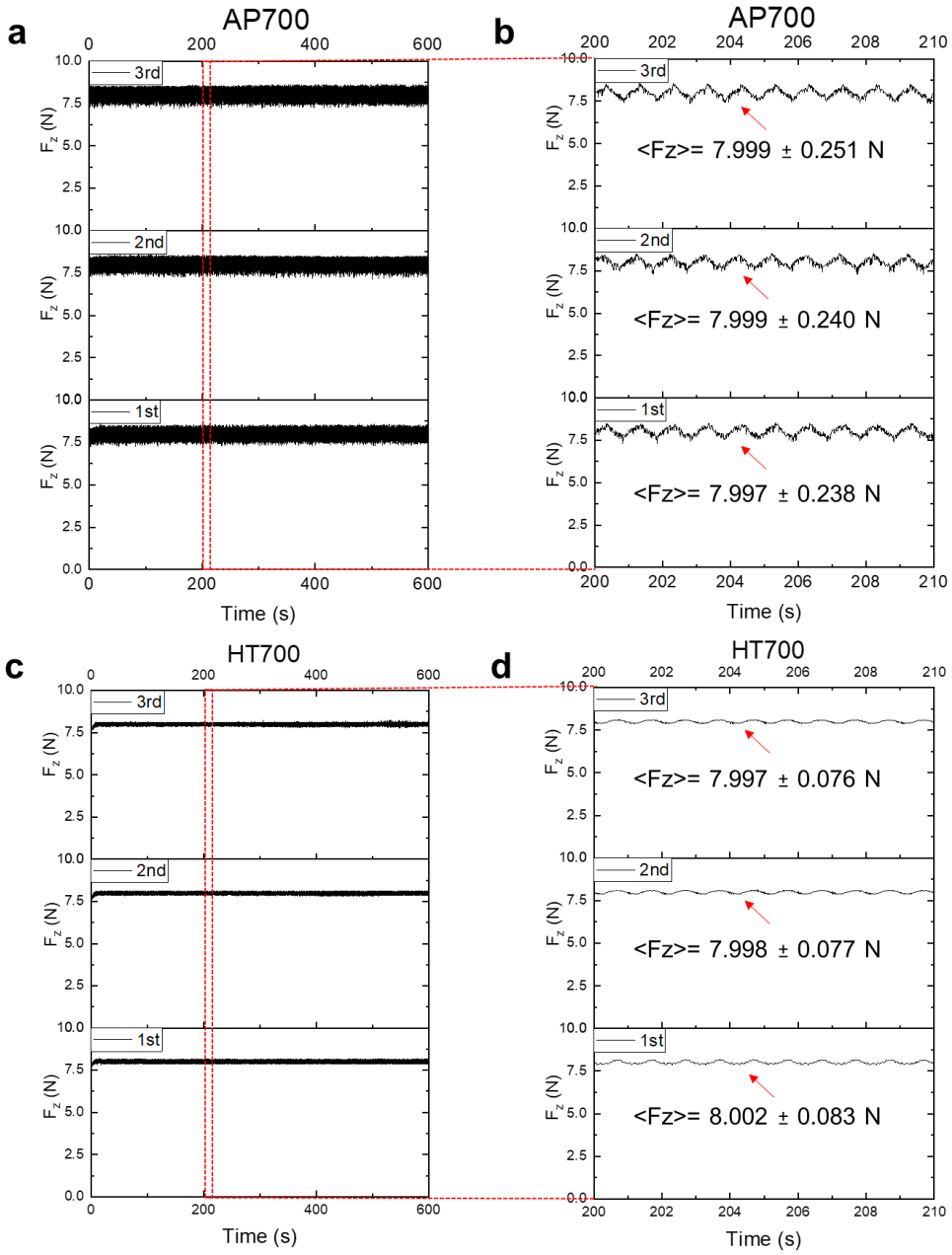

Supplementary Figure 10. Raw data of the frictional force (F_z). a,c Raw data (not processed by the RTECviewer software) of normal force (F_z, as defined in **Supplementary Figure 8a**) of AP700 and HT700. F_z from 200 to 210 seconds of **b** AP700 and **d** HT700 sample. Values in < > from **b, d** represent average values of F_z from the entire test (600 sec). 1st, 2nd, and 3 rd represents three repeated tests.

Using such raw data, COF (defined as the absolute value of F_x/F_z) of all samples are obtained (see **Supplementary Figure 11**). A closer examination shows that there is significant fluctuation of the COF values due to COF becoming very close to zero every time the motion changes direction, i.e. every 0.5 sec, as shown in **Supplementary Figure 12**.

For such raw data, the default RTECviewer software performs the treatment of F_x, F_z, and COF data according to eqn. 4 to minimize the effects of these near-zero values. For example, the force (F_x or F_z) at time t is processed as:

$$Force\_t\_mean = \frac{\int_{t-\delta t}^{t} Force\_t \times dt}{\delta t},\ \delta t = \frac{1}{2f} = 0.5\ sec \tag{4}$$

where Force_t is the raw data of force at time t, and Force_t_mean is the software processed force at time t. This data is plotted in the software by default, which we used to plot the original Figure 2 without knowing that it was processed. We verified using Python (see algorithm in the appendix) that using the raw F_x data of AP700 with a square-type waveform, the processed data indeed resembles a sine-type wave form, as shown in **Appendix Figure R3**.

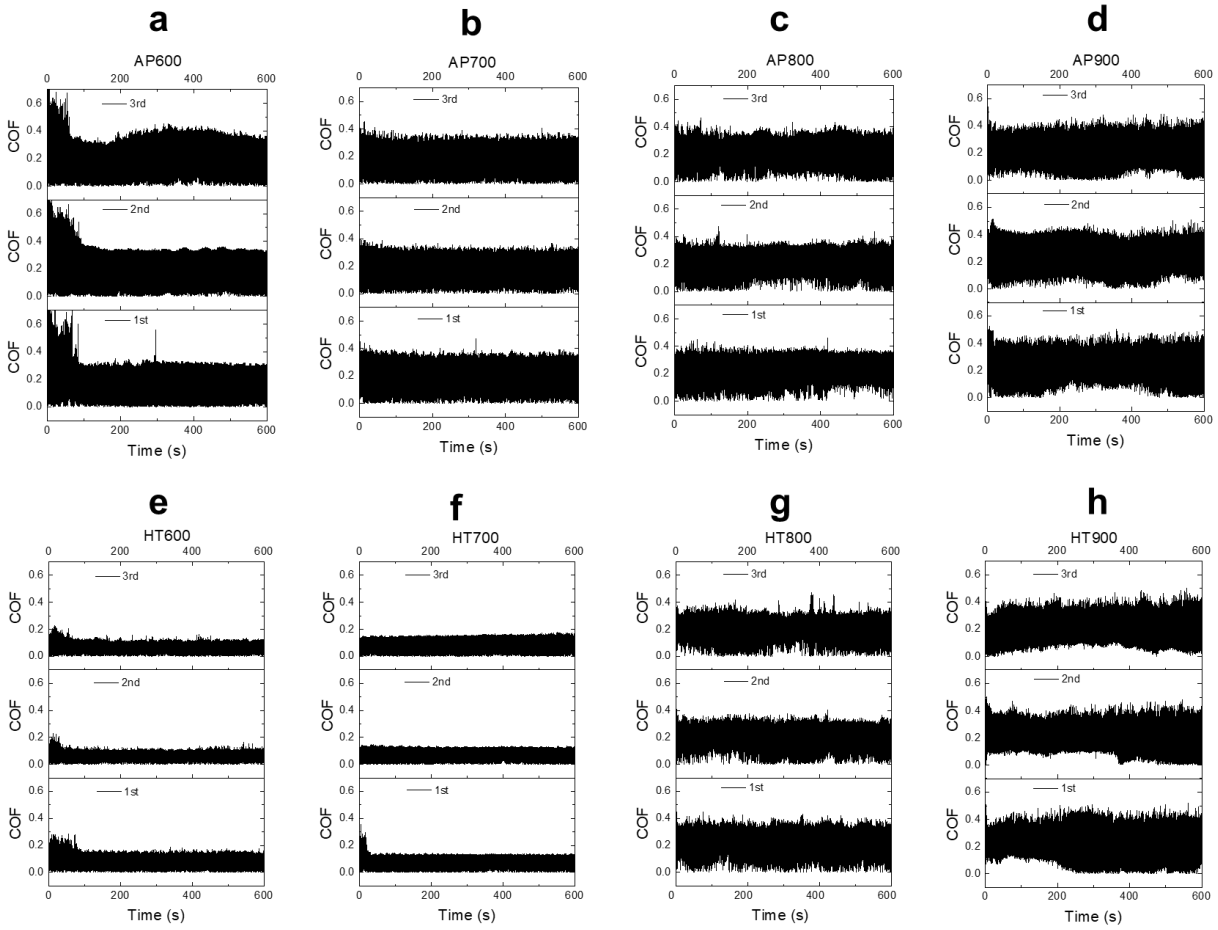

Supplementary Figure 11. Raw data of COF. a,c Raw data (not processed by the RTECviewer software) of COF of **a** AP600, **b** AP700, **c** AP800, **d** AP900, **e** HT600**, f** HT700, **g** HT800, and **h** HT900. 1st, 2nd, and 3rd represent three repeated tests.

Supplementary Figure 12 shows that such processed data smooths the raw COF curve for AP700. However, for HT700, whose raw COF shows little fluctuation, the amplitude of processed

data is even higher than the original raw data. For example, **Supplementary Figure 13b-c** shows that the amplitude of processed data is lower than that of raw data for AP700, AP900, and HT900 sample, but is higher than raw data for HT700. We also performed an analysis to evaluate whether such treatment affects the average value of COF. As shown in **Supplementary Figure 13a**, the difference between average COF between the raw and processed data is negligible for most samples (i.e. AP700, AP800, AP900, HT800, and HT900). However, it becomes noticeable for AP600, HT600, and HT700, likely due to their relatively high COF during the running-in period (see the first ~ 50 -100 sec of **Supplementary Figure 11a,e, and f)** so that of the average COF of the processed data is slightly higher than that of the raw data. For this reason, only raw data of F_x, F_z, and COF is used in the revised paper, including **Figures 1f,g,h,i and 2** of the main text.

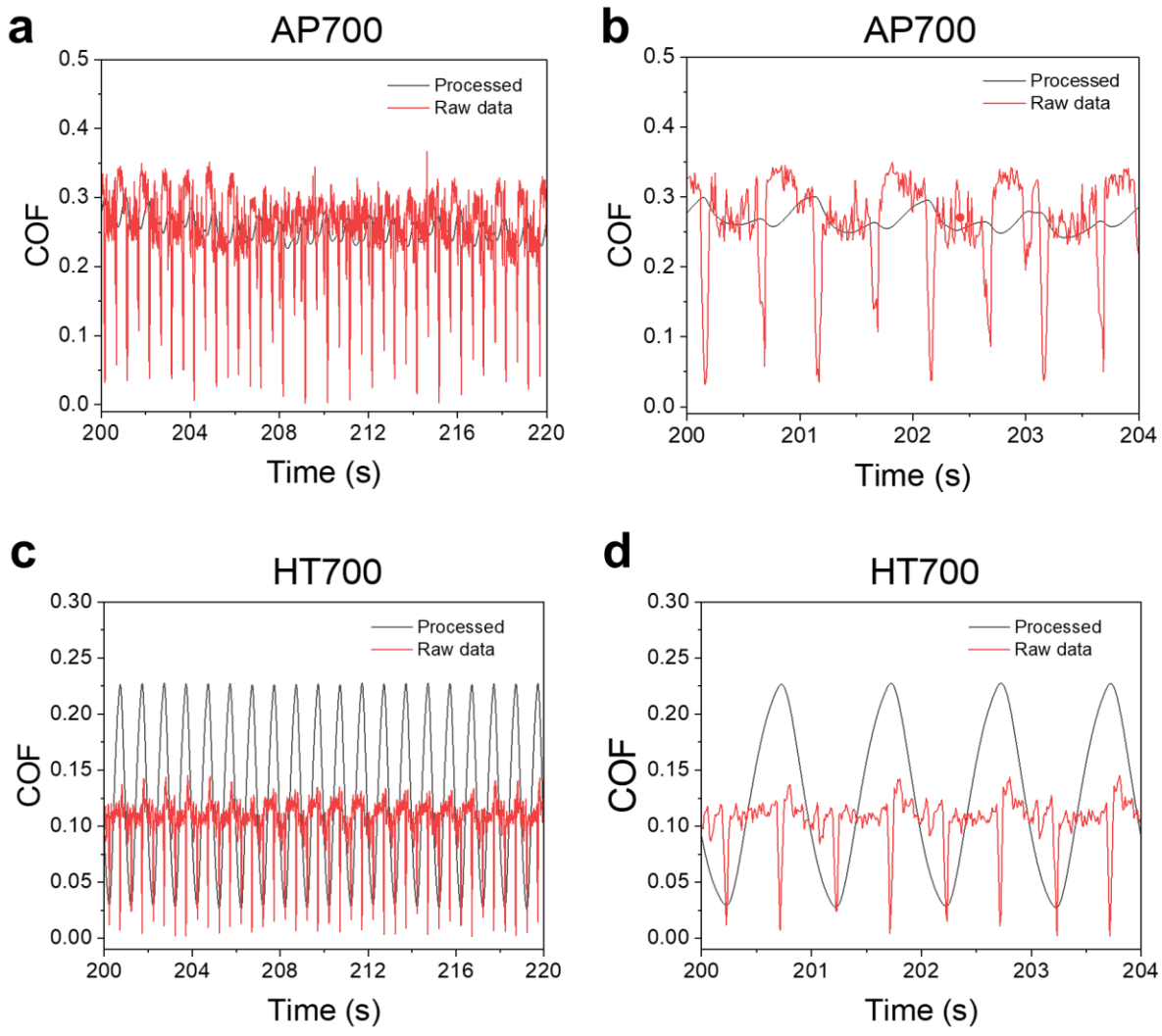

Supplementary Figure 12. Raw vs. processed data of COF. a,c Raw vs. processed COF data by the RTECviewer software of **a,b** AP700, and **c**,**d** HT700 near 200 sec.

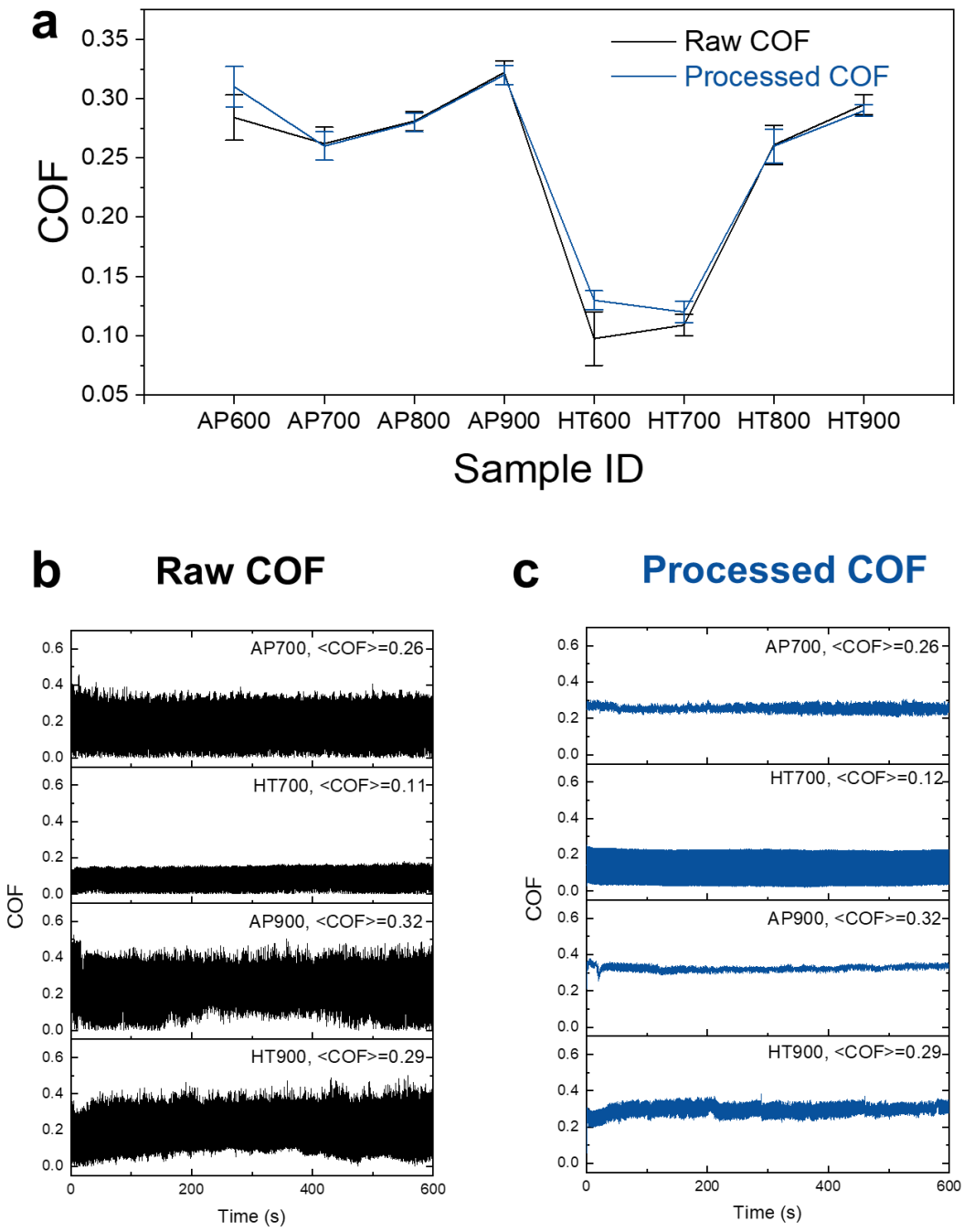

Supplementary Figure 13. Comparison of COF from raw vs. processed data. a Average COF from raw vs. processed data by the RTECviewer software for all samples. **b** Raw and **c** processed COF data for AP700, HT700, AP900, and HT900 samples.

Below is the revised Figure 2 in the main text. The raw COF data of all samples are now provided in the Source data file, as shown in the screenshot of Figure R2 below.

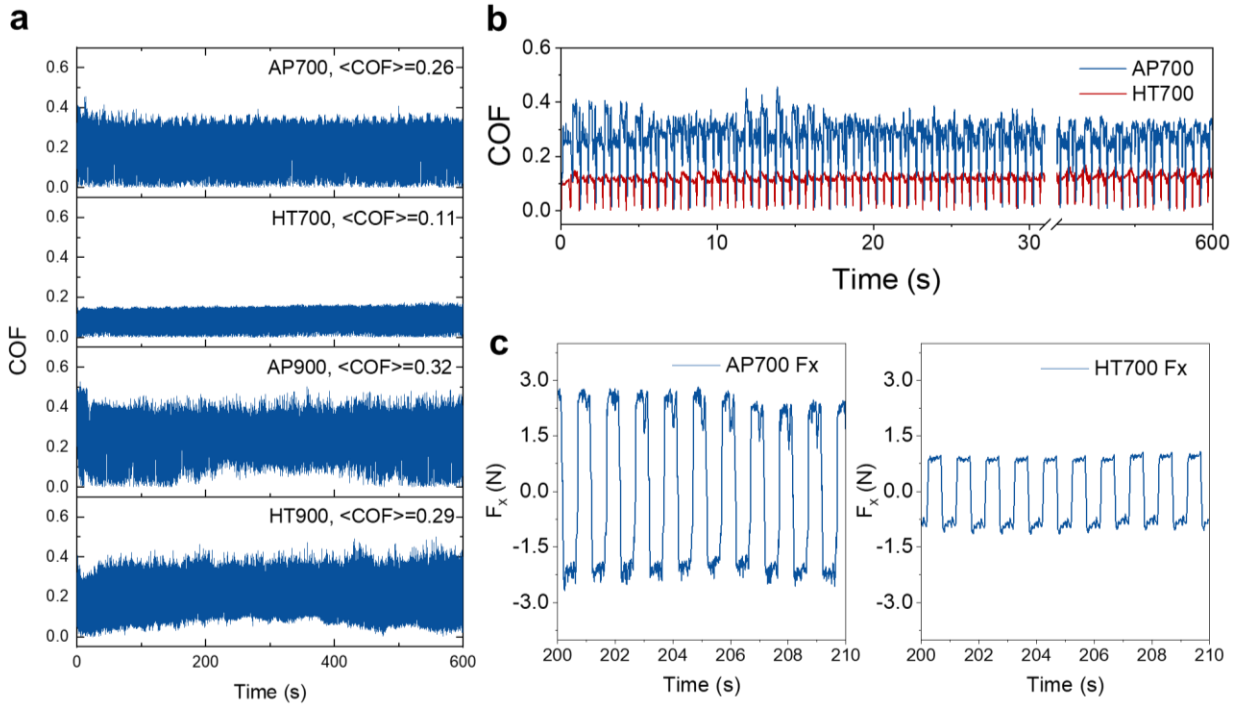

Figure 2. Temporal evolution of COF and friction force F_x. a COF of AP and HT samples from 700 and 900 ^oC. The unit of time is second (s). **b** COF of AP700 vs. HT700, **c** Frictional force (F_x) for AP700 and HT 700 samples from 200-210 s.

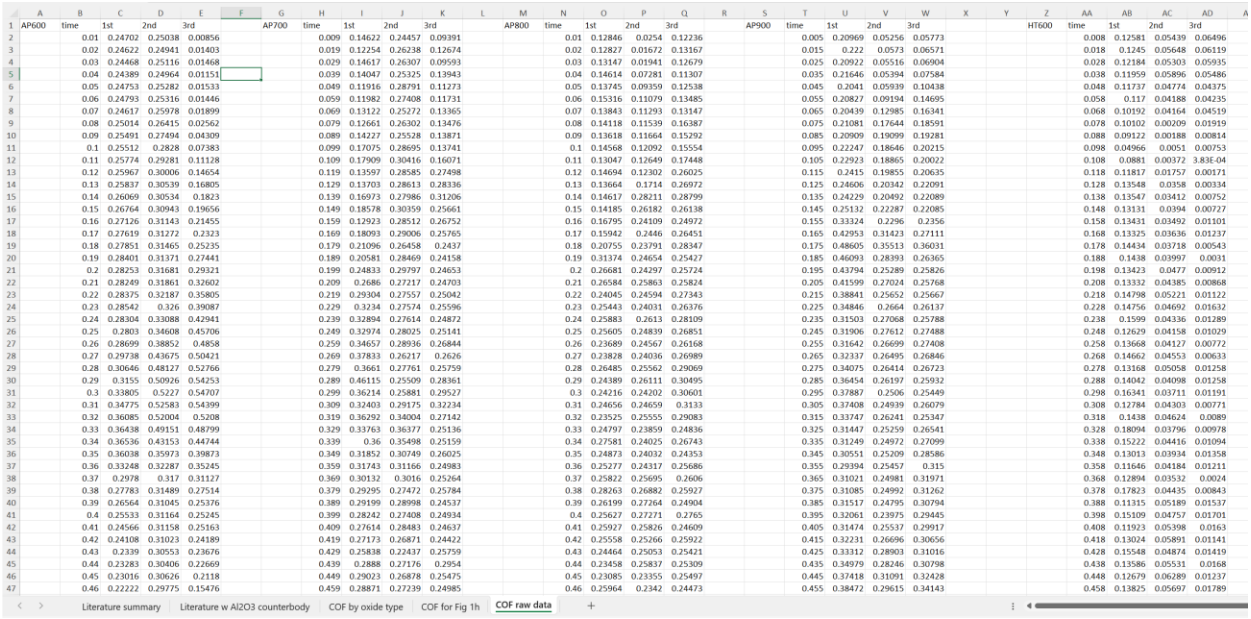

AP600	time	1st	2nd	3rd	AP700	time	1st	2nd	3rd	AP800	time	1st	2nd	3rd	AP900	time	1st	2nd	3rd	HT600	time	1st	2nd	3rd
	0.01	0.24702	0.25038	0.00856		0.009	0.14622	0.24457	0.09391		0.01	0.12846	0.0254	0.12236		0.005	0.20969	0.05256	0.05773		0.008	0.12581	0.05439	0.06496
	0.02	0.24622	0.24941	0.01403		0.019	0.12254	0.26238	0.12674		0.02	0.12827	0.01672	0.13167		0.015	0.222	0.0573	0.06571		0.018	0.1245	0.05648	0.06119
	0.03	0.24468	0.25116	0.01468		0.029	0.14617	0.26307	0.09593		0.03	0.13147	0.01941	0.12679		0.025	0.20922	0.05516	0.06904		0.028	0.12184	0.05303	0.05935
	0.04	0.24389	0.24964	0.01151		0.039	0.14047	0.25325	0.13943		0.04	0.14614	0.07281	0.11307		0.035	0.21646	0.05394	0.07584		0.038	0.11959	0.05896	0.05486
	0.05	0.24753	0.25282	0.01533		0.049	0.11916	0.28791	0.11273		0.05	0.13745	0.09359	0.12538		0.045	0.2041	0.05939	0.10438		0.048	0.11737	0.04774	0.04375
	0.06	0.24793	0.25316	0.01446		0.059	0.11982	0.27408	0.11731		0.06	0.15316	0.11079	0.13485		0.055	0.20827	0.09194	0.14695		0.058	0.117	0.04188	0.04235
	0.07	0.24617	0.25978	0.01899		0.069	0.13122	0.25272	0.13365		0.07	0.13843	0.11293	0.13147		0.065	0.20439	0.12985	0.16341		0.068	0.10192	0.04164	0.04519
	0.08	0.25014	0.26415	0.02562		0.079	0.12661	0.26302	0.13476		0.08	0.14118	0.11539	0.16387		0.075	0.21081	0.17644	0.18591		0.078	0.10102	0.00209	0.01919
	0.09	0.25491	0.27494	0.04309		0.089	0.14227	0.25528	0.13871		0.09	0.13618	0.11664	0.15292		0.085	0.20909	0.19099	0.19281		0.088	0.09122	0.00188	0.00814
	0.1	0.25512	0.2828	0.07383		0.099	0.17075	0.28695	0.13741		0.1	0.14568	0.12092	0.15554		0.095	0.22247	0.18646	0.20215		0.098	0.04966	0.0051	0.00753
	0.11	0.25774	0.29281	0.11128		0.109	0.17909	0.30416	0.16071		0.11	0.13047	0.12649	0.17448		0.105	0.22923	0.18865	0.20022		0.108	0.0881	0.00372	3.83E-04
	0.12	0.25967	0.30006	0.14654		0.119	0.13597	0.28585	0.27498		0.12	0.14694	0.12302	0.26025		0.115	0.2415	0.19855	0.20635		0.118	0.11817	0.01757	0.00171
	0.13	0.25837	0.30539	0.16805		0.129	0.13703	0.28613	0.28336		0.13	0.13664	0.1714	0.26972		0.125	0.24606	0.20342	0.22091		0.128	0.13548	0.0358	0.00334
	0.14	0.26069	0.30534	0.1823		0.139	0.16973	0.27986	0.31206		0.14	0.14617	0.28211	0.28799		0.135	0.24229	0.20492	0.22089		0.138	0.13547	0.03412	0.00752
	0.15	0.26764	0.30943	0.19656		0.149	0.18578	0.30359	0.25661		0.15	0.14185	0.26182	0.26138		0.145	0.25132	0.22287	0.22085		0.148	0.13131	0.0394	0.00727
	0.16	0.27126	0.31143	0.21455		0.159	0.12923	0.28512	0.26752		0.16	0.16795	0.24109	0.24972		0.155	0.33324	0.2296	0.2356		0.158	0.13431	0.03492	0.01101
	0.17	0.27619	0.31272	0.2323		0.169	0.18093	0.29006	0.25765		0.17	0.15942	0.2446	0.26451		0.165	0.42953	0.31423	0.27111		0.168	0.13325	0.03636	0.01237
	0.18	0.27851	0.31465	0.25235		0.179	0.21096	0.26458	0.2437		0.18	0.20755	0.23791	0.28347		0.175	0.48605	0.35513	0.36031		0.178	0.14434	0.03718	0.00543
	0.19	0.28401	0.31371	0.27441		0.189	0.20581	0.28469	0.24158		0.19	0.31374	0.24654	0.25427		0.185	0.46093	0.28393	0.26365		0.188	0.1438	0.03997	0.0031
	0.2	0.28253	0.31681	0.29321		0.199	0.24833	0.29797	0.24653		0.2	0.26681	0.24297	0.25724		0.195	0.43794	0.25289	0.25826		0.198	0.13423	0.0477	0.00912
	0.21	0.28249	0.31861	0.32602		0.209	0.2686	0.27217	0.24703		0.21	0.26584	0.25863	0.25824		0.205	0.41599	0.27024	0.25768		0.208	0.13332	0.04385	0.00868
	0.22	0.28375	0.32187	0.35805		0.219	0.29304	0.27557	0.25042		0.22	0.24045	0.24594	0.27343		0.215	0.38841	0.25652	0.25667		0.218	0.14798	0.05221	0.01122
	0.23	0.28542	0.326	0.39087		0.229	0.3234	0.27574	0.25596		0.23	0.25443	0.24031	0.26376		0.225	0.34846	0.2664	0.26137		0.228	0.14756	0.04692	0.01632
	0.24	0.28304	0.33088	0.42941		0.239	0.32894	0.27614	0.24872		0.24	0.25883	0.2613	0.28109		0.235	0.31503	0.27068	0.25788		0.238	0.1599	0.04336	0.01289
	0.25	0.2803	0.34608	0.45706		0.249	0.32974	0.28025	0.25141		0.25	0.25605	0.24839	0.26851		0.245	0.31906	0.27612	0.27488		0.248	0.12629	0.04158	0.01029
	0.26	0.28699	0.38852	0.4858		0.259	0.34657	0.28936	0.26844		0.26	0.23689	0.24567	0.26168		0.255	0.31642	0.26699	0.27408		0.258	0.13668	0.04127	0.00772
	0.27	0.29738	0.43675	0.50421		0.269	0.37833	0.26217	0.2626		0.27	0.23828	0.24036	0.26989		0.265	0.32337	0.26495	0.26846		0.268	0.14662	0.04553	0.00633
	0.28	0.30646	0.48127	0.52766		0.279	0.3661	0.27761	0.25759		0.28	0.26485	0.25562	0.29069		0.275	0.34075	0.26414	0.26723		0.278	0.13168	0.05058	0.01258
	0.29	0.3155	0.50926	0.54253		0.289	0.46115	0.25509	0.28361		0.29	0.24389	0.26111	0.30495		0.285	0.36454	0.26197	0.25932		0.288	0.14042	0.04098	0.01258
	0.3	0.33805	0.5227	0.54707		0.299	0.36214	0.25881	0.29527		0.3	0.24216	0.24202	0.30601		0.295	0.37887	0.2506	0.25449		0.298	0.16341	0.03711	0.01191
	0.31	0.34775	0.52583	0.54399		0.309	0.32403	0.29175	0.32234		0.31	0.24656	0.24659	0.3133		0.305	0.37408	0.24939	0.26079		0.308	0.12784	0.04303	0.00771
	0.32	0.36085	0.52004	0.5208		0.319	0.36292	0.34004	0.27142		0.32	0.23525	0.25555	0.29083		0.315	0.33747	0.26241	0.25347		0.318	0.1438	0.04624	0.0089
	0.33	0.36438	0.49151	0.48799		0.329	0.33763	0.36377	0.25136		0.33	0.24797	0.23859	0.24836		0.325	0.31447	0.25259	0.26541		0.328	0.18094	0.03796	0.00978
	0.34	0.36536	0.43153	0.44744		0.339	0.36	0.35498	0.25159		0.34	0.27581	0.24025	0.26743		0.335	0.31249	0.24972	0.27099		0.338	0.15222	0.04416	0.01094
	0.35	0.36038	0.35973	0.39873		0.349	0.31852	0.30749	0.26025		0.35	0.24873	0.24032	0.24353		0.345	0.30551	0.25209	0.28586		0.348	0.13013	0.03934	0.01358
	0.36	0.33248	0.32287	0.35245		0.359	0.31743	0.31166	0.24983		0.36	0.25277	0.24317	0.25686		0.355	0.29394	0.25457	0.315		0.358	0.11646	0.04184	0.01211
	0.37	0.2978	0.317	0.31127		0.369	0.30132	0.3016	0.25264		0.37	0.25822	0.25695	0.2606		0.365	0.31021	0.24981	0.31971		0.368	0.12894	0.03532	0.0024
	0.38	0.27783	0.31489	0.27514		0.379	0.29295	0.27472	0.25784		0.38	0.28263	0.26882	0.25927		0.375	0.31085	0.24992	0.31262		0.378	0.17823	0.04435	0.00843
	0.39	0.26564	0.31045	0.25376		0.389	0.29199	0.28998	0.24537		0.39	0.26199	0.27264	0.24904		0.385	0.31517	0.24795	0.30794		0.388	0.11315	0.05189	0.01537
	0.4	0.25533	0.31164	0.25245		0.399	0.28242	0.27408	0.24934		0.4	0.25627	0.27271	0.2765		0.395	0.32061	0.23975	0.29445		0.398	0.15109	0.04757	0.01701
	0.41	0.24566	0.31158	0.25163		0.409	0.27614	0.28483	0.24637		0.41	0.25927	0.25826	0.24609		0.405	0.31474	0.25537	0.29917		0.408	0.11923	0.05398	0.0163
	0.42	0.24108	0.31023	0.24189		0.419	0.27173	0.26871	0.24422		0.42	0.25558	0.25266	0.25922		0.415	0.32231	0.26696	0.30656		0.418	0.13024	0.05891	0.01141
	0.43	0.2339	0.30553	0.23676		0.429	0.25838	0.22437	0.25759		0.43	0.24464	0.25053	0.25421		0.425	0.33312	0.28903	0.31016		0.428	0.15548	0.04874	0.01419
	0.44	0.23283	0.30406	0.22669		0.439	0.2888	0.27176	0.2954		0.44	0.23458	0.25837	0.25309		0.435	0.34979	0.28246	0.30798		0.438	0.13586	0.05531	0.0168
	0.45	0.23016	0.30626	0.2118		0.449	0.29023	0.26878	0.25475		0.45	0.23085	0.23355	0.25497		0.445	0.37418	0.31091	0.32428		0.448	0.12679	0.06289	0.01237
	0.46	0.22222	0.29775	0.15476		0.459	0.28871	0.27239	0.24985		0.46	0.25964	0.2342	0.24473		0.455	0.38472	0.29615	0.34143		0.458	0.13825	0.05697	0.01789

Literature summary | Literature w Al2O3 counterbody | COF by oxide type | COF for Fig 1h | COF raw data

Figure R2. Screenshot of COF raw data for all samples.

In addition to updating the raw data in the revised manuscript, we also provide additional information about the tribometer setup and validation tests.

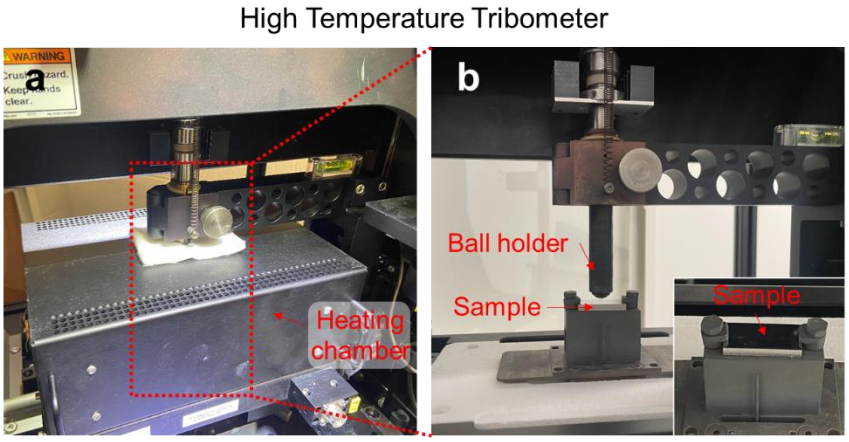

Supplementary Figure 6. Photographs of the high-temperature tribological tester (Rtec MFT-5000). a A close-up of the tester with the heating chamber installed. **b** A view of the ball holder and Inconel sample with the heating chamber removed. The inset in **b** shows a top-down view of the sample, secured by two side screws.

Supplementary Figure 6 shows the setup for the high temperature wear test, including a photo of the heating chamber and the sample mounting. To evaluate the test setup using the Rtec tribometer, we performed wear tests using stainless steel 316 coupons against Al_2O_3 ball. Tests were conducted at room temperature under ambient conditions, with a sliding speed of 20 mm/s and a Hertzian contact pressure of 1.59 GPa, replicating the conditions reported in Ref [12]. As

shown in **Supplementary Figure 7a,** the COF of stainless steel 316 against Al_2O_3 ball has an average value of 0.57, which agrees well with the value (COF=0.56) reported in Ref [12].

In addition, we also evaluated the extent of how counterbody material type affect the frictional response by performing wear test under the same conditions (i.e. sliding speed, Hertzian pressure) using tungsten carbide (WC) ball as counterbody. The results in **Supplementary Figure 7b** shows that a lower COF (COF=0.51) was obtained using WC counterbody than that using Al_2O_3 ball (COF=0.57). Based on these observations, we limit the literature data in Fig 1h to include only those using Al_2O_3 counter bodies.

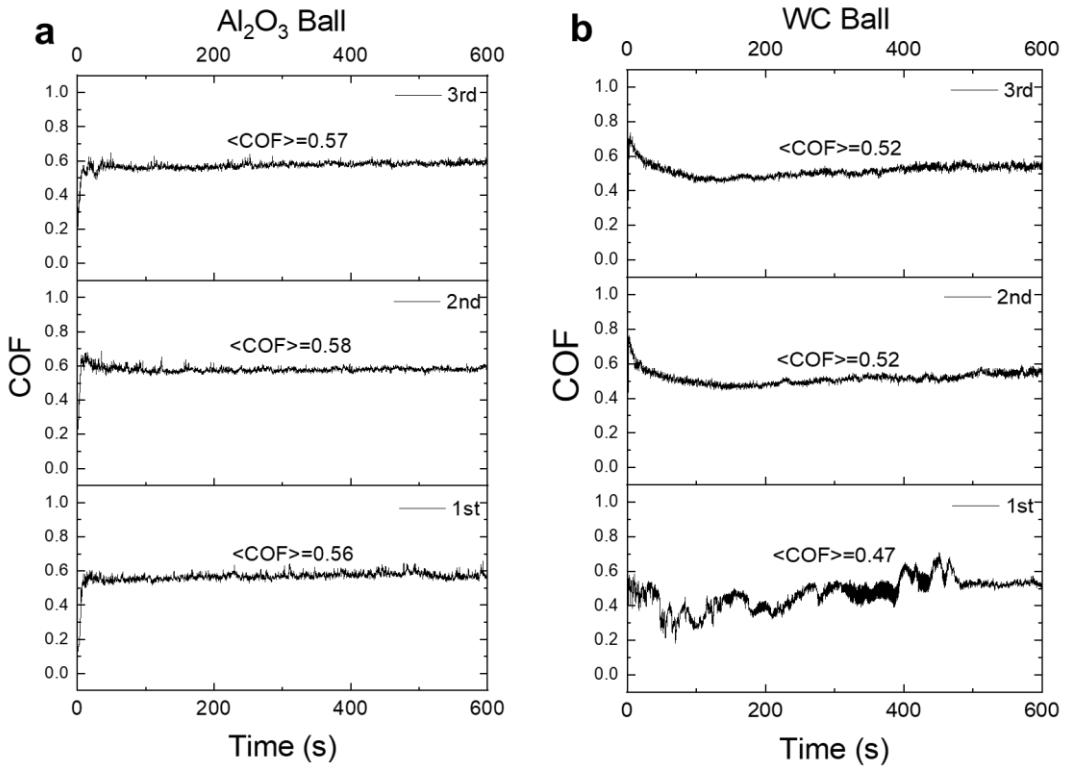

Supplementary Figure 7. Validation test results using two different counter bodies: (a) COF of stainless steel 316 against an Al_2O_3 ball and (b) COF against a WC ball. Tests were conducted at room temperature under ambient conditions, with a sliding speed of 20 mm/s and a Hertzian contact pressure of 1.59 GPa, replicating the conditions reported in Ref [12]. COF values presented in this figure are obtained after processing via RTECviewer software. See Supplementary Information section 3.3 for details.

Q2.2. In Fig 1i, the presentation of the results of this work compared to that of other reported coefficients of friction from the literature are misleading. The histograms of friction data are shown across a wide range of temperatures and different structures. Only one result from this work was reported. However, this one data point is picked off of the minimum of the friction waveform. The authors should justify this comparison as they are not comparing apples-to-apples.

Response: As mentioned in the previous question, we have revised this figure to focus exclusively on studies using Al_2O_3 as the counterbody. For the values presented in this work, we used the average COF for each sample. The COF values, including the average and standard deviation from the raw data, are summarized in Table R1 below. For instance, the HT700 sample has an average COF of 0.109 with a standard deviation of 0.009. As shown in **Figure R3**, the calculated average values accurately represent the COF during sliding, while the minimum COF, which occurs during the direction switch in the reciprocal wear test, is consistently close to zero.

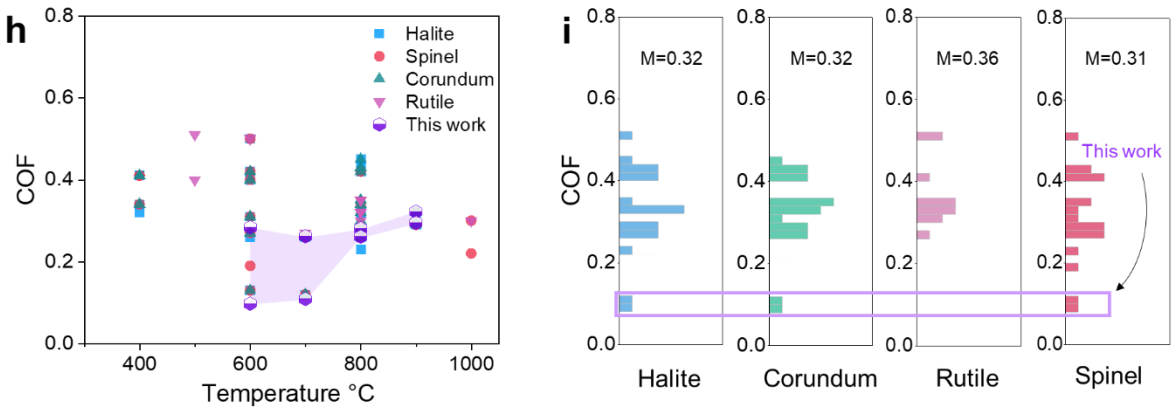

Figure 1. h. Summary of COF from literature using Al_2O_3 as counterbody (source data are provided as a Source Data file) and this work. For surface with more than one oxide type, all oxides are plotted as overlapping points in **h**. **i.** COF histogram of various oxides (halite, corundum, rutile, and spinel). M in **i** represent average value of the COF.

Table R1. Summary of average and standard deviation of raw COF data.

Temperature (°C)	HT		AP	
	<COF>	SD	<COF>	SD
600	0.0976	0.0226	0.284	0.0191
700	0.109	0.009	0.262	0.0139
800	0.261	0.0163	0.281	0.008
900	0.295	0.00859	0.322	0.01

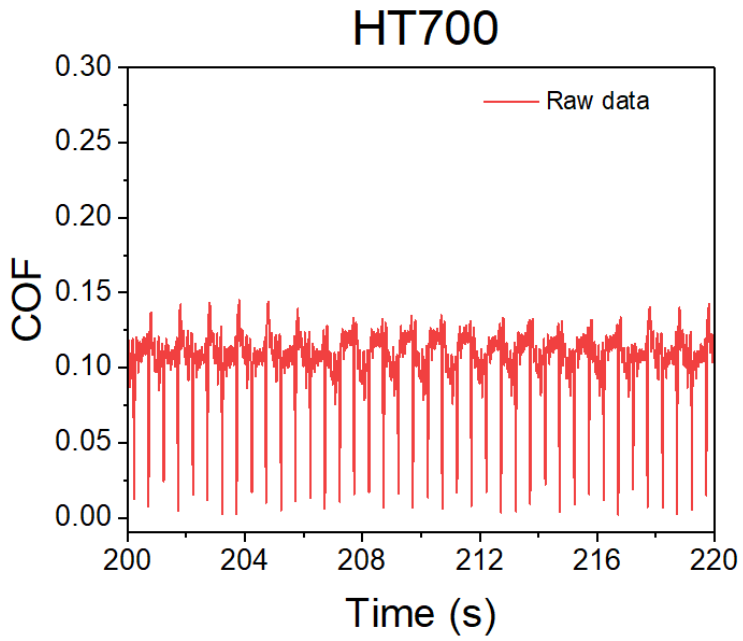

Figure R3. Raw data of COF for HT700 sample from time 200-220 sec.

Q2.3: The authors report an average friction coefficient of 0.12 with a standard deviation of 0.009 for sample HT700 (Pg 5, line 147). Figure 2 a,b shows the friction coefficient of this sample to vary between ~0.04 and 0.24, in a large waveform. How was the average and standard deviation of this measurement calculated? A variation between such a large range of friction coefficients should not result in a standard deviation as low as 0.009.

Response: COF mean values are first calculated for each of the three repeated tests. Then the average and standard deviation of COF is calculated based on these three measurements. Please refer to our previous discussion in question Q2.1. In the revised manuscript, we have used only the raw COF data, not the processed COF data. The raw COF data for all samples, including the three repeated tests for each, is now included in the Source Data file.

Q2.4. In the methods section, the authors state that all tests on the tribometer were carried out 3 times. The friction data shown in Fig 2 is the acquired data of one test. Was the extreme, cyclical variation observed for each test on sample HT700? How were the error bars shown for the COF data shown in Fig. 1f calculated? Again, a standard deviation value of 0.009 for a friction coefficient which varies 0.04-0.22 is not correct. Does this error bar reflect the standard deviation between the 3 separate tests performed?

Response: As stated in the previous question, the error bars are obtained from three repeated tests, not from one test. To briefly recap, we calculated the average COF from the 1st, 2nd, and 3rd test for each sample, and obtained three values of COF. Using these three values, the average and standard deviation of COF is obtained. Such data is shown in **Table R1**, and used to plot **Figure**

1f-i. In **Figure 2** of the paper, one of such test results are shown for each sample, and the three repeated results of all samples are shown in **Supplementary Figure 11**.

Q2.5: The friction power spectrum is just dropped in the paper and not really useful or discussed. Why?

Response: Thank you for the question. The power spectrums analysis was used to understand the presence or absence of self-organized criticality in the friction data [3-5]. Please see our detailed discussion of the power spectrum in the **response to Q1.7** from reviewer 1. In short summary, due to the lack of systematic study to separate the effects of stick-slip vs. phase transition on the change of power law exponent, we have removed such analysis from Figure 2.

Q2.6. While I am not an expert in DFT and cannot adequately assess the merits of it, it appears that the authors were able to predict which types of oxides could produce low friction interfaces – a novel and interesting contribution.

Response: Thank you for your favorable comments for our DFT work.

Q2.7. The issues with the friction results/reporting are significant and the results are not sufficient to support the claims made in this paper.

Response: Thank you for your criticism. We provided additional information from questions Q2.1-Q2.6 above to justify the revised results about the COF data, which support the claims of the paper.

Reviewer #3

Q3.1. Are there any surface oxide after the heat treatment? I assume there is some surface oxide as the specimen was air cooled from 954°C after solutionization (pg. 14, line 369). In that case, what is the thickness and nature of the oxide on the specimen before wear test? Without this data (XPS survey and high resolution scan of AP and HT surface, cross-sectional TEM/STEM), it is difficult to fully trace the structural origin and evolution of the lubricious spinel oxide. As it stands, it is not clear when the spinel oxide was first formed.

Response: Thank you for the valuable suggestion. As shown in **Figure R4** below, high-resolution XPS analysis comparing the unworn AP and HT samples provides insights into the valence states of Cr, Ni, and Fe. After C 1s calibration, the data reveals the presence of metal oxides in both AP and HT samples, likely originating from the metal powder, printing process, and heat treatment. Although both AP700 and HT700 samples contain spinel-structured oxides, as indicated by GI-XRD results in **Figure 3** of the paper, their oxide layer structures are markedly different. This suggests that bulk metal oxides does not significantly affect the observed differences in oxide layer structure.

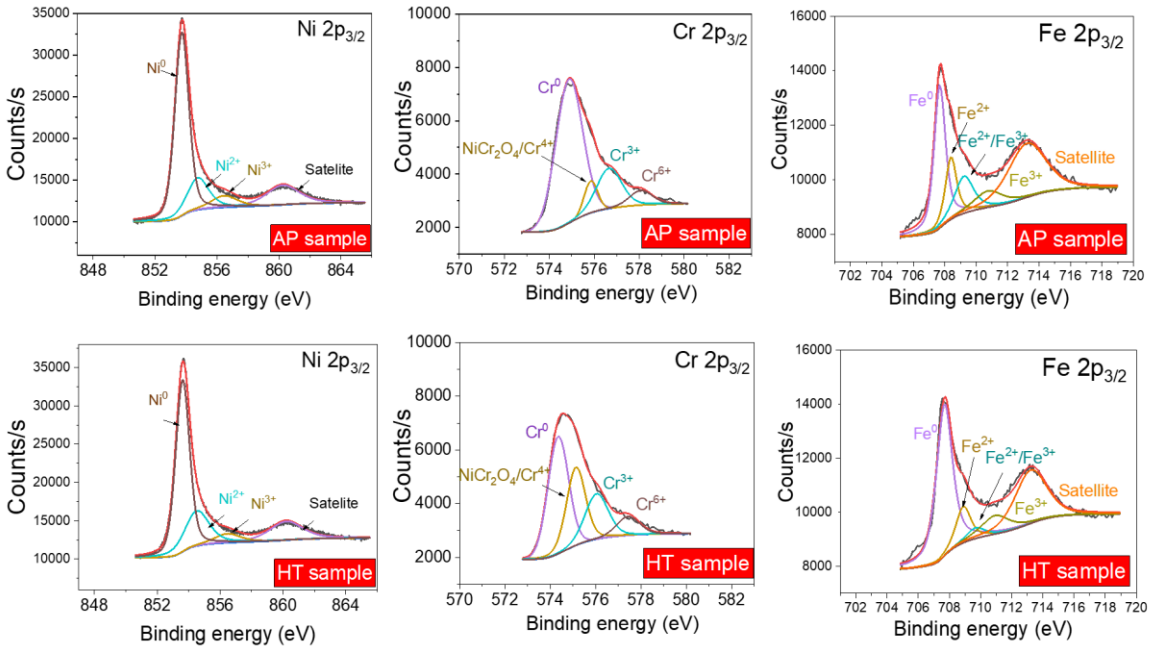

Figure R4. High resolution XPS spectra of Ni, Cr and Fe after 3 min of sputtering for AP and HT samples.

Q3.2. The microstructure of the surface oxide is not clearly shown in the STEM data and only dark contrast can be observed within the oxide layer on the HAADF images. For instance, what is the grain size of the surface oxide? Perhaps this can be addressed with bright field TEM imaging.

Response: We thank the reviewer for their suggestion. To visualize the grain size of the oxide layer, we created virtual bright field and annular dark field images from the 4D-STEM collected in the oxide layer that was used for the phase map constructions. We amend the main text on Page 9 to add the following results on the grain size, and to direct the readers to additional information in the Supplementary Information.

"... When the wear temperature increased from 700 °C to 900 ° C, the oxide microstructure clearly coarsened, as shown in the phase maps (Fig. 4d) and in virtual bright field and annular dark field images of HT700 and HT900 (Supplementary Figure 27). The oxide structure of HT900 can be viewed as corundum structured oxide particles of ~ 50-200 nm embedded in the matrix of coarse tetragonal and monoclinic spinel oxide phases of similar sizes, whereas the oxide structure of HT700 consists of smaller ~ 5-30 nm grains. ..."

We add the following text to the Supplementary Information regarding the creation of these virtual images:

"To provide additional insight into the typical grain sizes of the HT700 and HT900 samples, we created virtual bright field and annular dark field reconstructions from the 4D-STEM data collected in the oxide regions of the two samples. An integration range of 0-3 mrad was used to construct the virtual bright field images and 15-38 mrad was used to construct the virtual annular dark field images. We find that the feature sizes in the phase maps in Fig. 4(c, d) are consistent with the grain sizes observed with these virtual images. From the 1 x 1 μm^2 virtual images, we identify the grain size in the HT700 sample to be on the order of 5-30 nm and in the HT900 sample to be on the order of 50-200 nm."

Q3.3. How does the grain size of the surface oxide layer compare to the size of the features on the phase map presented in Figure 4?

Response: We appreciate the reviewer for initiating this point of discussion. Since the virtual images are constructed using the same 4D-STEM data used for the phase maps, we can directly relate the feature sizes from the images and phase maps. In the virtual bright field and annular dark field STEM images shown in the **Supplementary Figure 27**, we have indicated with red dashed boxes the regions which exactly correspond with the phase maps shown in the main text (Figure 4). We show that overall, the feature size in the phase maps is consistent with the grain sizes observed with these virtual images: the grain sizes of the HT700 and HT 900 samples being on the order of 5-30 nm and 50-200 nm, respectively. We updated the manuscript accordingly.

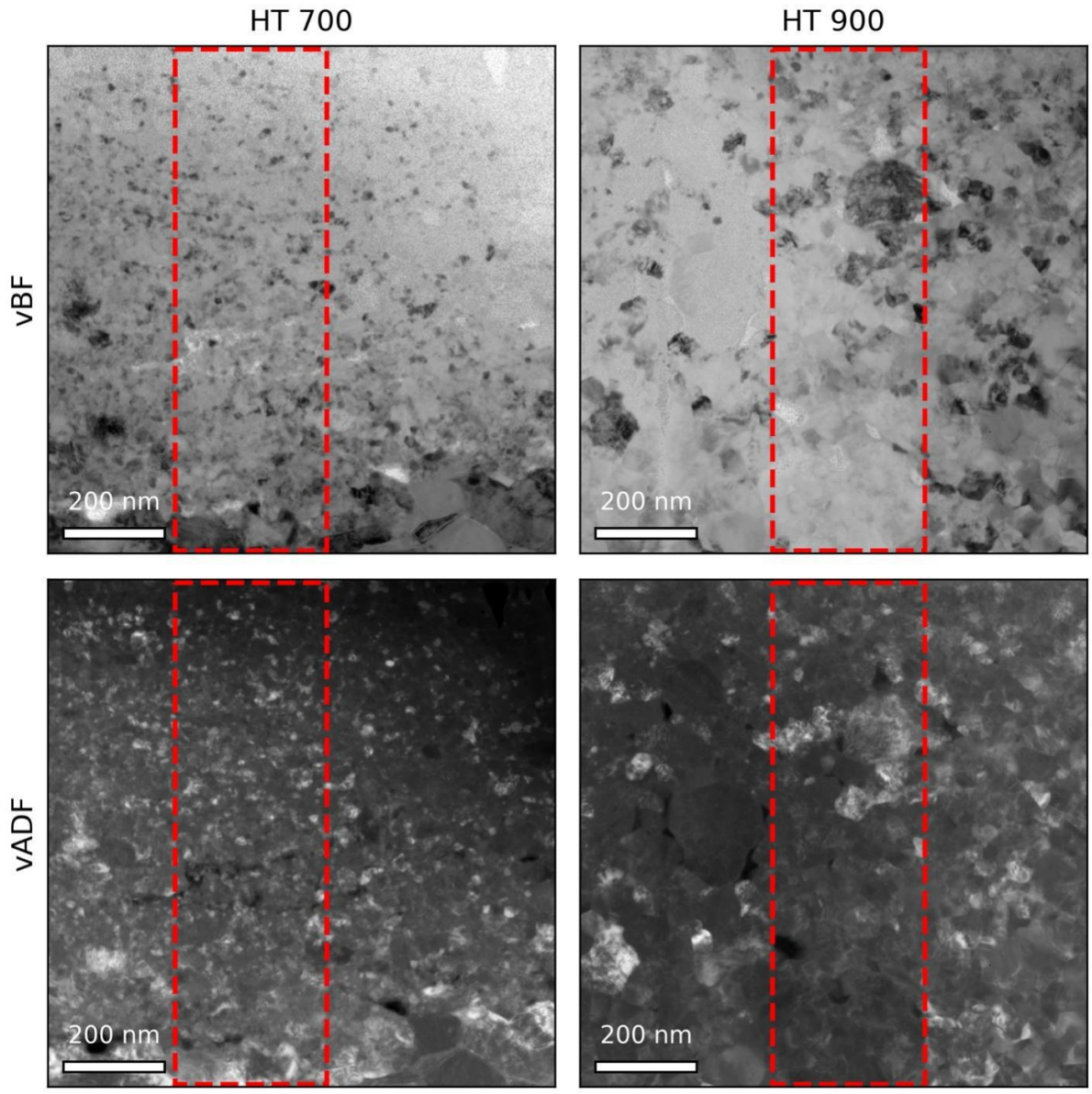

Supplementary Figure 27. Virtual bright field and annular dark field reconstructed STEM images of the oxide regions of the HT700 and HT900 cross-sectional samples highlighting the difference in apparent grain size between the samples. The regions associated with the phase maps in Fig. 4(c, d) are indicated with red dashed boxes.

Q3.4. Pg 15, line 425, it should be Transmission electron microscopy and diffraction simulation

Response: Thank you for catching this mistake. This is corrected now.

Q3.5. Pg 15, line 427, .. using four-dimensional scanning transmission electron microscopy (4D-STEM)

Response: This is corrected now.

Q3.6. In standard practice of XPS, survey scans should be included for the reader better comprehend the high resolution XPS scans of the material under investigation.

Response: The XPS survey scans are provided below, which is also included in the **Supplementary Figure 23** now.

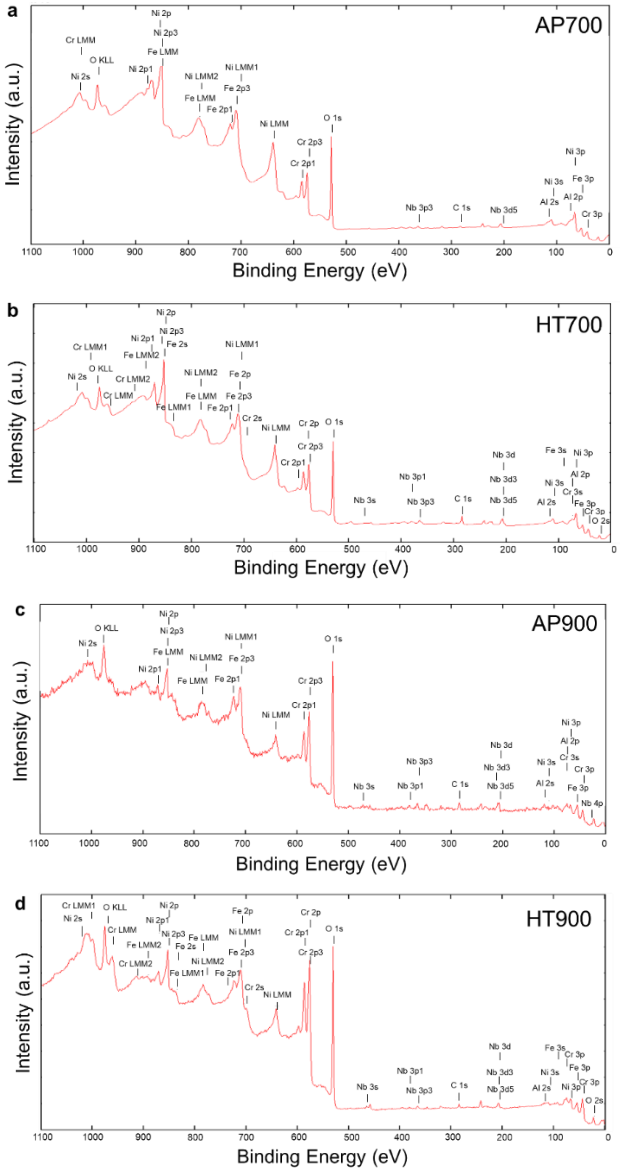

Supplementary Figure 23. XPS survey profile of Inconel 718 samples (a) AP700, (b) HT700, (c) AP900, and (d) HT900.

Reviewer #4

Q4.1. I co-reviewed this manuscript with one of the reviewers who provided the listed reports. This is part of the Nature Communications initiative to facilitate training in peer review and to provide appropriate recognition for Early Career Researchers who co-review manuscripts.

Response: Thank you for reviewing our work.

References

[1] J.F. Archard, Contact and Rubbing of Flat Surfaces, Journal of Applied Physics 24(8) (1953) 981-988.
[2] F. Stott, The role of oxidation in the wear of alloys, Tribology International 31(1-3) (1998) 61-71.
[3] P. Bak, C. Tang, K. Wiesenfeld, Self-organized criticality: An explanation of the 1/f noise, Physical review letters 59(4) (1987) 381.
[4] F.R. Zypman, J. Ferrante, M. Jansen, K. Scanlon, P. Abel, Evidence of self-organized criticality in dry sliding friction, Journal of Physics: Condensed Matter 15(12) (2003) L191.
[5] S.V. Buldyrev, J. Ferrante, F.R. Zypman, Dry friction avalanches: Experiment and theory, Physical Review E 74(6) (2006) 066110.
[6] W. Hu, Y. Ge, Q. Xu, R. Huang, Q. Zhao, H. Gou, M. McSaveney, C. Chang, Y. Li, X. Jia, High time-resolved studies of stick–slip show similar dilatancy to fast and slow earthquakes, Proceedings of the National Academy of Sciences 120(47) (2023) e2305134120.
[7] J.W. Yu, S. Rahbari, T. Kawasaki, H. Park, W.B. Lee, Active microrheology of a bulk metallic glass, Science Advances 6(29) (2020) eaba8766.
[8] M. Duarte, J. Molina, R. Prieto, E. Louis, J. Narciso, Self-similar fluctuations and 1/f noise in dry friction dynamics, Metallurgical and Materials Transactions A 38 (2007) 298-305.
[9] M. Duarte, I. Vragovic, J. Molina, R. Prieto, J. Narciso, E. Louis, 1/f noise in sliding friction under wear conditions: The role of debris, Physical review letters 102(4) (2009) 045501.
[10] M.F. Ashby, S.C. Lim, Wear-mechanism maps, Scripta Metallurgica et Materialia 24(5) (1990) 805-810.
[11] G. Wood, T. Hodgkiess, The hardness of oxides at ambient temperatures, Materials and Corrosion 23(9) (1972) 766-773.
[12] R.A. García-León, J. Martínez-Trinidad, A. Guevara-Morales, I. Campos-Silva, U. Figueroa-López, Wear Maps and Statistical Approach of AISI 316L Alloy under Dry Sliding Conditions, J Mater Eng Perform 30(8) (2021) 6175-6190.

==========**Appendix: Python code for the RTECviewer algorithm** ==========

```
import pandas as pd
import numpy as np
import matplotlib.pyplot as plt

# Load the CSV file of raw data
file_path = 'AP700_Fx_1st.csv'  # Update the file path as needed
data = pd.read_csv(file_path)

# Extract the relevant columns
time = data['Timestamp'].values
force = data['Fx-Processed'].values

# Initialize an array to store the smoothed force values
smoothed_force = np.zeros_like(force)

# Implement the smoothing algorithm for the past 0.5 seconds
for i in range(1, len(force)):
    # Determine the time window to average over (past 0.5 seconds)
    t_start = time[i] - 0.5
    # Select the indices that fall within the past 0.5 seconds
    indices = np.where((time >= t_start) & (time <= time[i]))[0]
    # Integrate (sum) force values over this time interval and divide by 0.5 to
get the average
    smoothed_force[i] = np.sum(force[indices] * np.diff(time[indices],
prepend=t_start)) / 0.5

# Plot the original and smoothed data with a focus on the 200 to 202 second
interval
plt.figure(figsize=(14, 7))
plt.plot(time, force, label='Original Fx-Processed')
plt.plot(time, smoothed_force, label='Smoothed Fx-Processed', color='red')
plt.xlim(200, 202)  # Set the x-axis limits to zoom in from 200 to 202 seconds
plt.xlabel('Timestamp')
plt.ylabel('Force')
plt.title('Original vs Smoothed Force Data (0.5s Average, 200-202s)')
plt.legend()
plt.grid(True)
plt.show()
```

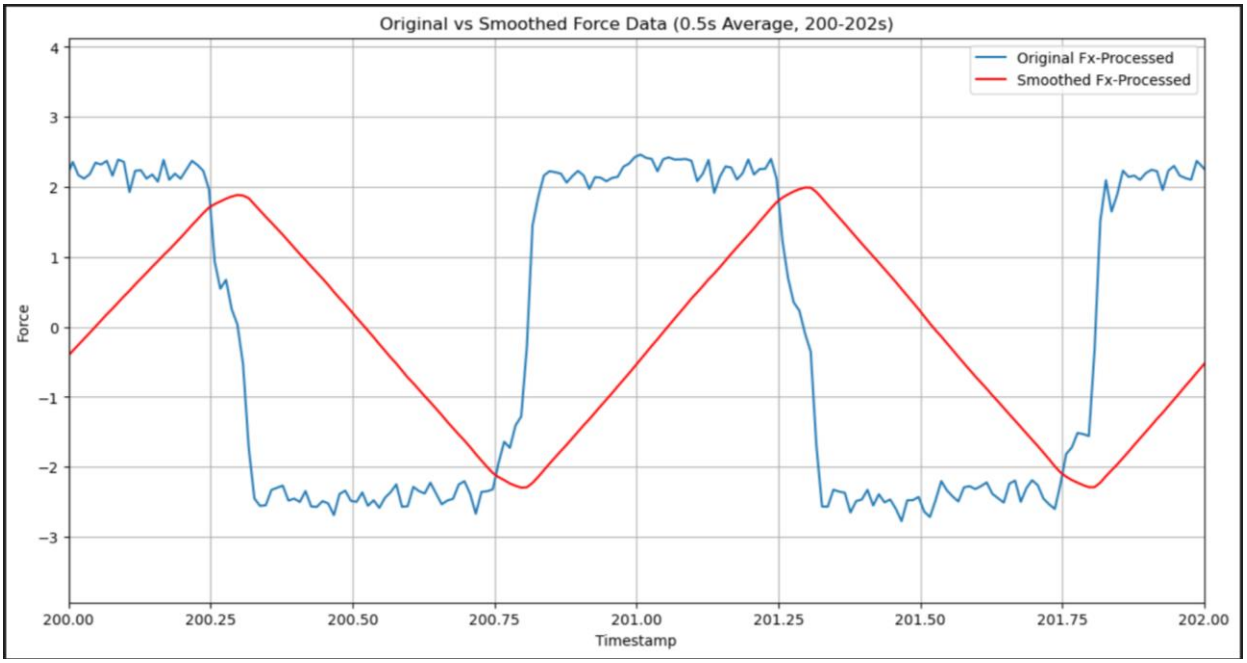

Figure R3. Plot generated using the Python code above to duplicate the RTECviewer algorithm, which convert the raw Fx data (blue curve) into the smoothed Fx data (red curve).

Response to Reviewer Comments (NCOMMS-24-09031A)

We sincerely thank all reviewers for the careful reading of our revised manuscript and for their constructive feedback. We provided below a detailed response to all the points raised in the reviewers' comments. Revisions made to the manuscript appear highlighted in yellow for ease of visualization.

Revisions made are highlighted below:

1. All corrections including the texts and figures are made per the instructions in the Author checklist.
2. Typos pointed out by Reviewer #3 is fixed.

Reviewer #1:

Comment: The revised paper "Spinel Oxide Enables High-Temperature Self-Lubrication in Superalloys" with reference number NCOMMS-24-09031A is focused on investigating the high temperature sliding friction and wear behaviour of SLM produced Inconel 718, in as-printed and heat treated conditions, during sliding against Al2O3. The overall aim of the study is to demonstrate that friction and wear control can be achieved by in-situ oxidation of a metal surface to facilitate formation of spinel-based oxide layers.

The Authors have made a very thorough job with addressing all the comments and questions raised by the Reviewer. The additional high temperature hardness measurements, in-depth analysis of the Al2O3 counter-body (SEM/EDS, XPS) after the tribological tests, and the detailed analysis and explanation of the friction data has significantly improved the quality of the manuscript. The Reviewer particularly appreciates the comprehensive and pedagogical explanations/justifications provided by the authors in the Response to Reviewers Comments.

With the implementation of all these changes, the Reviewer considers the manuscript to be acceptable for publication.

Authors' response: We sincerely thank the reviewer for the positive feedback on our revised manuscript. We also appreciate the time and effort the reviewer has dedicated to reviewing our work, which has been invaluable in helping us improve the quality and clarity of our paper.

Reviewer #3

Question. The authors have addressed all of my comments with the exception of Q3.4. Pg 15, line 425, it should be Transmission electron microscopy and diffraction simulation. (pg 16, line 455 on the revised manuscript)

Authors' response: We have fixed this.